primary antibody (anti-V5 [1:1000], anti-caspase-14 [1:5000] and anti-α-tubulin [1:200] antibody) for 2 h at room temperature, followed by incubation with horseradish peroxidase (HRP)-conjugated appropriate secondary antibody, and the proteins were detected using an enhanced chemiluminescence system (Amersham Biosciences, Piscataway, NJ, USA) according to the manufacturer's instructions.

TUNEL staining

Transferase deoxytidyl uridine end labeling (TUNEL) staining was performed with ApopTag apoptosis detection kit (Intergen, Burlington, MA, USA) exactly as described previously.[18] HaCaT cells on coverslips were fixed with −20°C methanol, rinsed with phosphate buffered saline (PBS) two times, and treated with 10% normal goat serum for 10 min. They were then incubated with the anti-V5 antibody for 30 min, rinsed with PBS three times, and incubated with biotin-conjugated goat antimouse IgG (Sigma, St Louis, MO, USA) for 30 min, followed by incubation with streptavidin–Cy3 conjugate (Sigma) for 30 min. Cells were incubated with working strength TdT enzyme at 37°C for 1 h, extensively washed with stop/wash buffer and PBS, and incubated with anti-digoxigenin conjugate fluorescent dye for 30 min. They were mounted on a glass slide with PermaFluor (Thermo-Shandon, Vernon Hills, IL, USA) and observed by confocal laser microscope (Olympus).

DNA fragmentation assay

After 48 h of transfection, HaCaT cells were lysed in lysis buffer (10 mmol/L Tris-HCl (pH 8.0), 100 mmol/L NaCl, 1% SDS, 1 mmol/L ethylene diamine tetra acetate, and 2 mg/mL proteinase K) for 1 h at 65°C. Following two successive extractions with phenol/chloroform, the DNA samples were precipitated in ethanol. After washing with 70% ethanol, the DNA samples were resuspended in TE buffer and subjected to 2% agarose gel electrophoresis.

Statistics

All values are presented as means ± standard error of the mean. The significance of the difference from the respective controls for each experiment test condition was assayed using a Student's *t*-test for each paired experiment. An ANOVA was used to test for significance ($P < 0.05$).

RESULTS

Subcellular localization of WT and mutant loricrin

Genomic DNA containing the coding region of WT loricrin and mutant loricrin was subcloned into pcDNA3.1/V5-His vector. The most frequent mutation, 730insG, was chosen for this study. The transfection efficiencies for WT and mutant loricrin were almost the same. Immunoblot analysis using anti-V5 antibody revealed that WT loricrin (Fig. 1a, arrow, 35 kDa) and mutant loricrin (arrowhead, 42 kDa) were expressed to almost the same degree (Fig. 1a). Although the expected molecular mass of WT loricrin is 35 kDa, the migrating position of WT loricrin was around the 37-kDa molecular marker. We think this migration is due to many aliphatic amino acids (glycine/serine/cystein) in WT loricrin. Next, to determine whether mutant loricrin protein localizes in the nucleus in cultured keratinocytes as in keratinocytes of loricrin keratoderma *in vivo*,[7] we transfected HaCaT cells with V5-tagged WT loricrin or mutant loricrin, the mutation in loricrin keratoderma, and stained them with an anti-V5 antibody and an anti-keratin antibody. WT loricrin distributes in the cytoplasm and nucleus (Fig. 1b, upper right panel). Mutant loricrin, which is predicted to get a nuclear localization signal, seems to localize in the nucleolus (Fig. 1c, upper right panel). Why it localizes in the nucleolus, rather than nucleus, is not clear as reported by Ishida-Yamamoto *et al.*[21] We analyzed 4 000 000 cells and found that transfection efficiency was the same in either semi-confluent or non-confluent state. That is, transfection efficiency was not dependent on confluency. When WT loricrin was transfected, we observed cells shrinking perhaps due to PCD.

Differentiation level of the HaCaT cells transfected with WT or mutant loricrin

At first, we transfected WT loricrin and mutant loricrin into normal human epidermal keratinocytes. Normal human epidermal keratinocytes were purchased from KURABO (Osaka, Japan). These primary human epidermal keratinocytes were cultured and transfected as described by DiColandrea *et al.*[22] However, we could not transfect WT and mutant loricrin constructs into normal human epidermal keratinocytes. That was

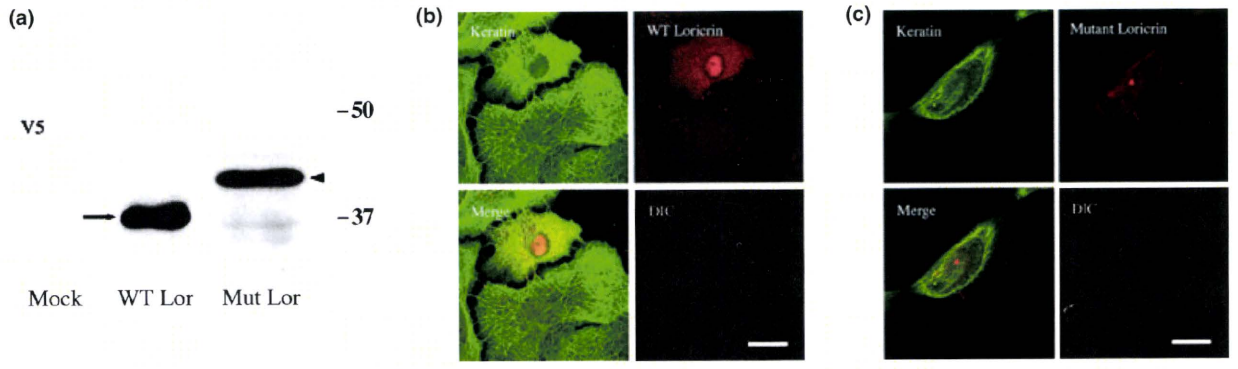

Figure 1. (a) Immunoblot analysis of wild-type (WT) loricrin-transfected HaCaT cells and mutant loricrn-transfected HaCaT cells. Immunoblot with anti-V5 antibody revealed that WT loricrin and mutant loricrin were expressed to almost the same degree. Arrow denotes 35-kDa WT loricrin including V5 tag sequence. Arrowhead denotes 42-kDa mutant loricrin including V5 tag sequence. Although the expected molecular mass of WT loricrin is 35 kDa, the migrating position of WT loricrin was around the 37-kDa molecular marker. We think this migration is due to many aliphatic amino acids (glycine/serine/cystein) in WT loricrin. (b,c) Distribution of WT loricrin-V5 and mutant loricrin-V5 of transfected HaCaT keratinocytes. HaCaT keratinocytes were transfected with either plasmid pcDNA3.1/V5-His-WT loricrin or plasmid pcDNA3.1/V5-His-mutant loricrin. Cells were fixed at 48 h post-transfection, and the fate of the transfected gene product was examined by double-label immunofluorescence. To visualize the transfected gene product, cells were stained with a mouse monoclonal antibody recognizing the sequence of V5. Antibody staining was followed by biotin-conjugated antimouse immunoglobulin G and Cy3-conjugated streptavidin. (b) Double-stainings of HaCaT cells with 1:100-diluted anti-V5 antibody (red) and 1:100-diluted anti-keratin antibody (green). WT loricrin distributes diffusely in the cytoplasm and in the nuclei in transfected cells. (Scale bars: 25 μm.) (c) Double-stainings of HaCaT cells with 1:100-diluted anti-V5 antibody (red) and 1:100-diluted anti-keratin antibody (green). Mutant loricrin distributes in the nucleolus as a V5-positive immunoreactive granule. (Scale bars: 25 μm.) DIC, differential interference contrast.

to say, transfection efficiency was so low (<0.1%) that we could not detect WT or mutant loricrin with immunoblot analysis. Then, we decided to use HaCaT cells. The HaCaT keratinocyte cell line is a spontaneously transformed human epithelial cell line derived from adult skin which maintains full epidermal differentiation capacity.[23] The transfection efficiency into HaCaT cells was approximately 3%. Because the expression of WT and mutant loricrin is observed only in morphologically different keratinocytes, we tried to estimate the differentiation level of WT and mutant loricrin transfected HaCaT cells. WT loricrin-transfected HaCaT cells exhibited positive immunoreactivities for periplakin, envoplakin, involucrin, transglutaminase 1 and filaggrin. Mutant loricrin-transfected HaCaT cells also exhibited positive immunoreactivities for periplakin, envoplakin, involucrin, transglutaminase 1 and filaggrin. Mutant loricrin in the nucleoli co-localized with periplakin, envoplakin, involucrin, transglutaminase 1 and filaggrin (Fig. 2). We could not transfect WT or mutant loricrin into non-differentiated level HaCaT cells (filaggrin-negative HaCaT cells). These results suggest that HaCaT cells expressing WT or mutant loricrin are at differentiation level because periplakin, envoplakin, involucrin, transglutaminase 1 and filaggrin are differentiation markers.

PCD and activation of caspases-14 in HaCaT cells expressing WT loricrin

To explore whether WT loricrin induces PCD in HaCaT cells, we first examined the effects of WT loricrin on cell morphology. Forty-eight hours after transfection, the number of cell deaths was determined by counting 10 000 HaCaT cells under a phase-contrast microsocpe. PCD cells were judged by staining both PCD nuclei with SYTO 13 and plasma-membrane permeabilization with Trypan blue. When WT loricrin was transfected, PCD cells which contained PCD nuclei were increased (Fig. 3a). PCD cells in 10 000 cells increased from 9 ± 2.2 of mock to 103 ± 4.3 of WT loricrin. In contrast, mutant loricrin did not increase PCD cells (8 ± 4.1 cells).

Furthermore, positive TUNEL stainings were observed in the nuclei in WT loricrin-transfected cells (Fig. 3b). Data from the DNA fragmentation assay showed that only WT loricrin induced DNA ladders

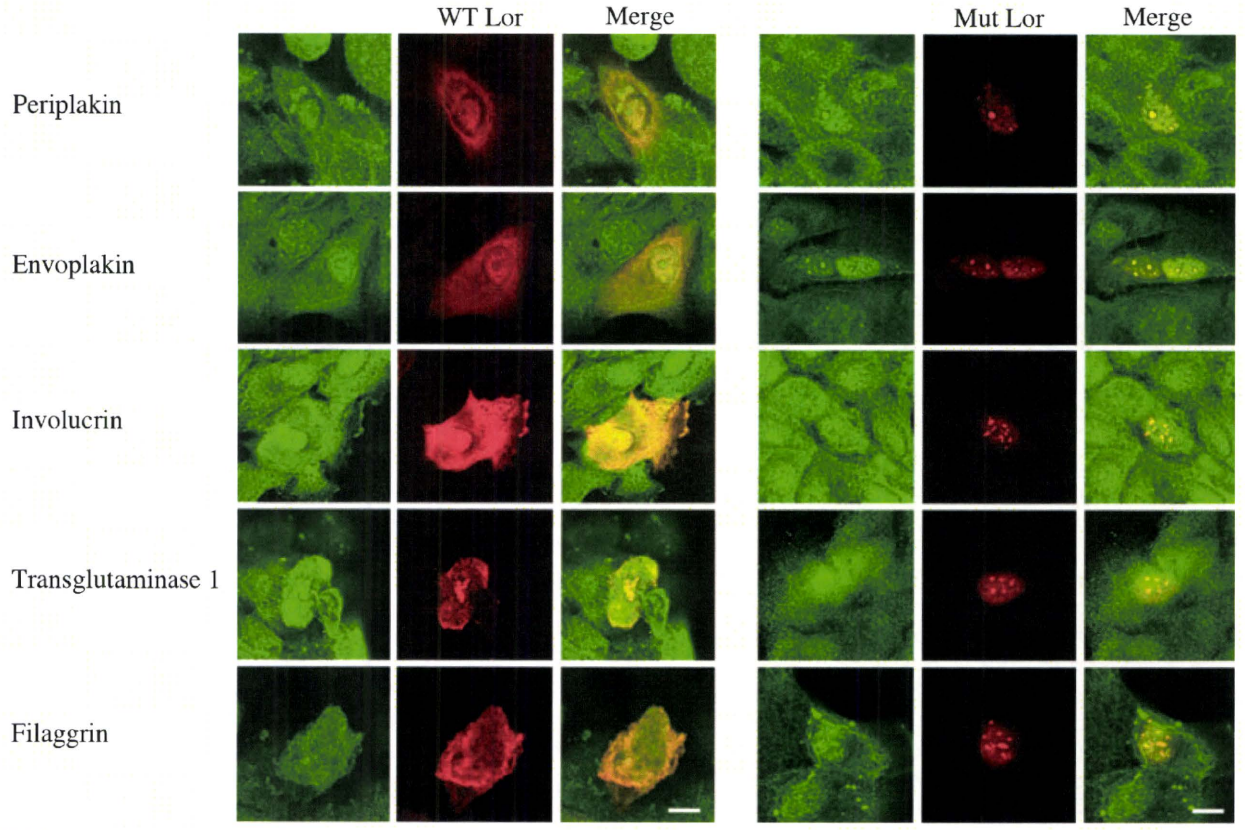

Figure 2. Differentiation level of the HaCaT cells after transfection of wild-type (WT) and mutant loricrin. WT loricrin-transfected HaCaT cells exhibited positive immunoreactivities for periplakin, envoplakin, involucrin, transglutaminase 1 and filaggrin. Mutant loricrin-transfected HaCaT cell also exhibited positive immunoreactivities for periplakin, envoplakin, involucrin, transglutaminase 1 and filaggrin. We could not transfect WT or mutant loricrin into non-differentiated level HaCaT cells (filaggrin-negative HaCaT cells). (Scale bars: 25 μm.)

(Fig. 3c). Immunoblot analysis using anti-caspase-14 antibody revealed that processing the p11 fragment was observed only in WT loricrin-transfected cells (Fig. 3d, arrow). Caspase-14 was not activated in mock or mutant loricrin-transfected HaCaT cells.

DISCUSSION

As far as we know, we showed for the first time that procaspase-14 was processed and activated accompanying PCD when we transfected WT loricrin in HaCaT cells. In contrast, transient expression of mutant loricrin in HaCaT keratinocytes does not result in PCD or activation of casapse-14. The number of PCD cells in cells transfected with WT loricrin was markedly higher than that in cells of transfected mock or mutant loricrin. In addition, we showed positive TUNEL staining in WT loricrin-transfected cells. Although we demonstrated that PCD occurred in the HaCaT cells after transient transfection of WT loricrin, we assume that this response represents a tissue-specific form of PCD that differs from classical apoptosis. The frame-shift mutations in the loricrin gene have produced mutant forms of loricrin with altered and extended COOH termini, as a consequence of alternative, downstream termination signals. Thus, the common feature of all loricrin mutations described to date is replacement of the COOH-terminal Gly- and Gln/Lys-rich domain with highly charged Arg- and Leu-rich domain amino acid sequences. Because the COOH-terminus of mutant loricrin is very different from the WT loricrin, namely, acquiring a nuclear localization signal, mutant loricrin accumulates in the nucleus. Mutant loricrin overexpressed in HaCaT cells by transfection did not cause PCD *in vitro*, which might be related to pathogenesis of

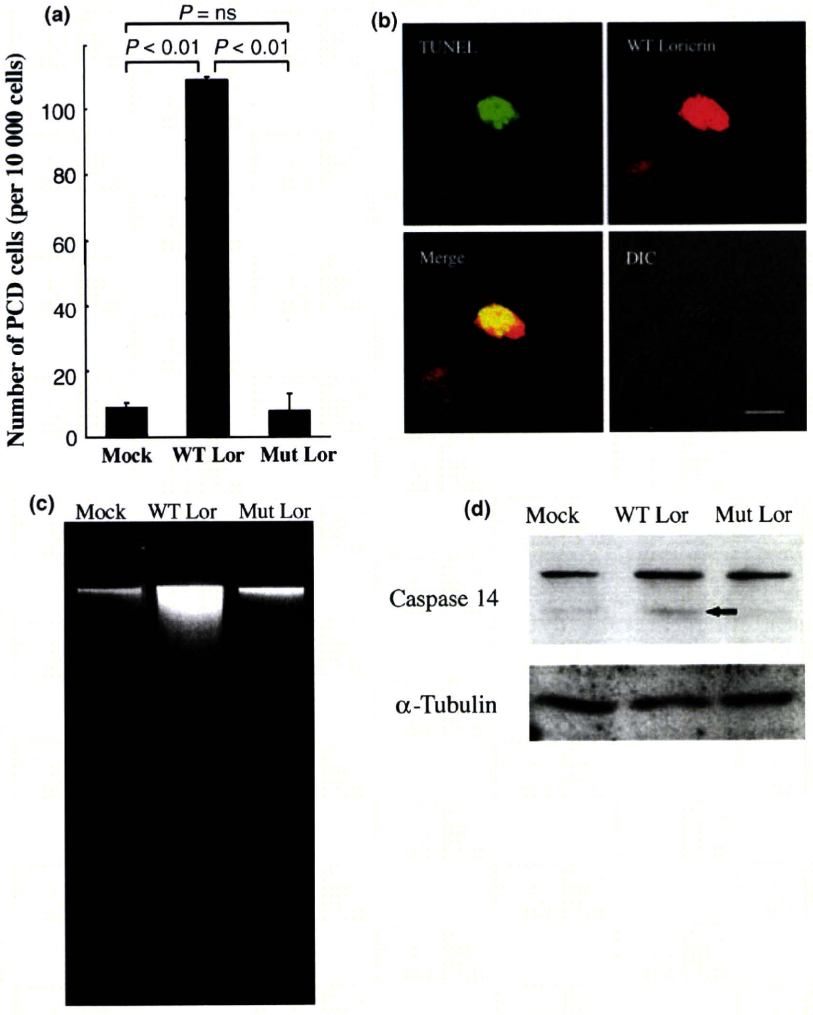

Figure 3. Induction of programmed cell death (PCD) by wild-type (WT) loricrin but not by mutant loricrin. (a) Number of PCD cells was significantly higher in WT loricrin than in mock or mutant loricrin (morphology) (n = 5). Quantification of PCD was performed by both staining PCD nuclei with SYTO 13 and plasma-membrane permeabilization with Trypan blue. (b) Double-stainings with 1:100-diluted anti-V5 antibody (red; upper right panel) and transferase deoxytidyl uridine end labeling (TUNEL) staining (green; upper left panel). Lower left panel shows merge of the two stainings. Positive TUNEL stainings were observed in the nuclei in WT loricrin-transfected cells. (Scale bars: 25 μm.) (c) Data from the DNA fragmentation assay showed that only WT loricrin induced DNA ladders. (d) Activation of caspase-14 by WT loricrin. Immunoblot with 1:5000 diluted anti-caspase-14 and with 1:200 diluted anti-α-tubulin antibody. Caspase-14 was activated in WT loricrin-transfected cells. Similar data were obtained in five experiments. DIC, differential interference contrast.

keratoderma although more studies are needed. Ishida-Yamamoto *et al.*[16] reported that number of TUNEL-positive cells was increased in the skin of loricrin keratoderma. They reported that epidermal differentiation in loricrin keratoderma seemed to be disrupted at the very late stages, immediately before the disintegration of apoptotic nuclei containing profilaggrin amino-terminus. Anti-apoptotic protein, such as Mcl-1, might be expressed more abundantly in HaCaT cells than *in vivo* epidermis because HaCaT cells were spontaneously immortalized an aneuploid human keratinocyte cell line.[24]

Filaggrin is an intermediate filament-associated protein that aggregates epidermal keratin filaments *in vitro* and is thought to perform a similar function during terminal differentiation *in vivo*. Loricrin and filaggrin are two major proteins expressed by terminally differentiated epidermal keratinocytes. Recently,

the importance of filaggrin has been underscored by demonstrating that loss-of-function mutations in the profilaggrin gene underlie the skin disease ichthyosis vulgaris, and that they strongly predispose to atopic dermatitis and asthma.[25,26] Dale *et al.*[27] showed that transient expression of filaggrin in epithelial cells led cell contraction, nuclear membrane breakdown and nuclear condensation. Dale *et al.*[27] and Kuechle *et al.*[28] stated that a low transfection rate is also seen in filaggrin constructs (<2%) as we observed with WT and mutant loricrin constructs. They reported that green fluorescent protein (GFP) and β-galactosidase control constructs showed 15–20% transfection rate. We also observed that the transfection rate of pcDNA3.1/V5-His WT keratin 14 was 20–30%. We also tried Lipofectamine 2000 (Invitrogen) as a transfection reagent. However, transfection efficiency of loricrin was almost the same as using LipofectAMINE plus reagent (Invitrogen). The reason why there is disparity in transfection rate between loricrin and keratin 14 constructs is not currently clear. In addition, we could not detect proteins by immunoblot analysis after transfection of WT and mutant loricrin constructs into cultured normal human epidermal keratinocytes. Similarly, we observed a cystatin A expression vector with cytomegalovirus immediate early promoter could not transfect cystatin A in cultured normal human epidermal keratinocytes.[29] Transfection of cornified cell envelope component proteins such as loricrin, filaggrin or cystatin A into cultured keratinocytes may be very difficult.

We formerly showed that no alterations could be observed in mice with an approximately twofold overexpression of human WT loricrin.[3] We also observed that human cystatin A transgenic mice did not show any abnormalities in the epidermis or hair follicle.[29] Presland *et al.*[30] created human filaggrin transgenic mice and observed no abnormalities in the epidermis, hair structures or tissue organization. Interestingly enough, there was no evidence of altered keratin filament organization in the suprabasal layers of filaggrin transgenic epidermis. On the contrary to these transgenic mice *in vivo* data, we observed that WT loricrin-transfected HaCaT keratinocytes were susceptible to PCD. Dale *et al.*[27] proved that transient transfection of epidermal filaggrin efficiently aggregates keratin filaments when expressed *in vitro* either in rat keratinocytes (keratin5/keratin14 and keratin1/keratin10) or monkey COS-7 cells (keratin8/keratin18). Presland *et al.*[30,31] reported that there was a disruption of cell–cell adhesion in keratinocytes overexpressing filaggrin, which they did not observe in transgenic mice overexpressing filaggrin. They speculated that cultured cells might be more sensitive to keratin filament disruption than epidermal tissue, which expressed a greater diversity of keratin proteins and thus contained a more robust intermediate filament network with stronger cell–cell adhesion through desmosomes. Similarly, we think cultured HaCaT cells may be more sensitive to various PCD stimuli than *in vivo* epidermal tissue which express a greater diversity of keratin proteins and contain an abundant type I keratin proteins that are known to prevent apoptosis.

Although the bulk of WT loricrin exists within keratohyalin granules and cornified cell envelope, WT loricrin is also known to be present in the nucleus at *in vivo* epidermis.[4] We also confirm that WT loricrin distributes in the nucleus *in vitro* transfected HaCaT cells. However, the function of WT loricrin is not known yet. The profilaggrin N-terminal domain localizes to both cytoplasm and nucleus of epidermal granular layer cells. Profilaggrin is a large phosphoprotein that is expressed in the granular cells of epidermis where it is localized in keratohyalin. It consists of multiple copies of single filaggrin units plus N- and C-terminal sequences that differ from filaggrin. The N-terminal sequence of human profilaggrin comprises two distinct domains; an acidic A domain of 81 amino acids that binds calcium, and a cationic B domain of 212 residues. The cellular distribution of WT loricrin is similar to that of profilaggrin N-terminal domain. We speculate that WT loricrin may interact with profilaggrin N-terminal domain *in vivo* and that this interaction may have some role in normal epidermal keratinization. To explore the expression of nuclear WT loricrin in cultured keratinocytes and epidermis and examine its association with profilaggrin N-terminal domain would be of great interest as a future project.

In summary, this study shows that expression of WT loricrin in HaCaT keratinocytes causes PCD whereas mutant loricrin is unable to cause PCD. Our results may implicate novel function of WT loricrin considering that the overexpression of filaggrin and profilaggrin results in PCD in both simple epithelial cells (COS-7) and rat epidermal keratinocyte cell line (REK).[27]

ACKNOWLEDGMENTS

We are grateful to Dr N. Fusenig for HaCaT cells; F. Naruse, T. Takamura and F. Nishiyama for technical assistance and artwork. This work was in part supported by grants from the Ministries of Health, Labor and Welfare and Education, Culture, Sports, Science, and Technology of Japan.

REFERENCES

1 Yoneda K, Hohl D, McBride OW *et al.* The human loricrin gene. *J Biol Chem* 1992; **267**: 18060–18066.
2 Yoneda K, McBride OW, Korge BP, Kim IG, Steinert PM. The cornified cell envelope: loricrin and transglutaminases. *J Dermatol* 1992; **19**: 761–764.
3 Yoneda K, Steinert PM. Overexpression of human loricrin in transgenic mice produces a normal phenotype. *Proc Natl Acad Sci USA* 1993; **90**: 10754–10758.
4 Ishida-Yamamoto A, Hohl D, Roop DR, Iizuka H, Eady RA. Loricrin immunoreactivity in human skin: localization to specific granules (L-granules) in acrosyringia. *Arch Dermatol Res* 1993; **285**: 491–498.
5 Ishida-Yamamoto A. Loricrin keratoderma: a novel disease entity characterized by nuclear accumulation of mutant loricrin. *J Dermatol Sci* 2003; **31**: 3–8.
6 Bickenbach JR, Greer JM, Bundman DS, Rothnagel JA, Roop DR. Loricrin expression is coordinated with other epidermal proteins and the appearance of lipid lamellar granules in development. *J Invest Dermatol* 1995; **104**: 405–410.
7 Maestrini E, Monaco AP, McGrath JA *et al.* A molecular defect in loricrin, the major component of the cornified cell envelope, underlies Vohwinkel's syndrome. *Nat Genet* 1996; **13**: 70–77.
8 Korge BP, Ishida-Yamamoto A, Punter C *et al.* Loricrin mutation in Vohwinkel's keratoderma is unique to the variant with ichthyosis. *J Invest Dermatol* 1997; **109**: 604–610.
9 Armstrong DK, McKenna KE, Hughes AE. A novel insertional mutation in loricrin in Vohwinkel's Keratoderma. *J Invest Dermatol* 1998; **111**: 702–704.
10 Takahashi H, Ishida-Yamamoto A, Kishi A, Ohara K, Iizuka H. Loricrin gene mutation in a Japanese patient of Vohwinkel's syndrome. *J Dermatol Sci* 1999; **19**: 44–47.
11 Matsumoto K, Muto M, Seki S *et al.* Loricrin keratoderma: a cause of congenital ichthyosiform erythroderma and collodion baby. *Br J Dermatol* 2001; **145**: 657–660.
12 O'Driscoll J, Muston GC, McGrath JA, Lam HM, Ashworth J, Christiano AM. A recurrent mutation in the loricrin gene underlies the ichthyotic variant of Vohwinkel syndrome. *Clin Exp Dermatol* 2002; **27**: 243–246.
13 Gedicke MM, Traupe H, Fischer B, Tinschert S, Hennies HC. Towards characterization of palmoplantar keratoderma caused by gain-of-function mutation in loricrin: analysis of a family and review of the literature. *Br J Dermatol* 2006; **154**: 167–171.
14 Ishida-Yamamoto A, McGrath JA, Lam H, Iizuka H, Friedman RA, Christiano AM. The molecular pathology of progressive symmetric erythrokeratoderma: a frameshift mutation in the loricrin gene and perturbations in the cornified cell envelope. *Am J Hum Genet* 1997; **61**: 581–589.
15 Ishida-Yamamoto A, Takahashi H, Iizuka H. Loricrin and human skin diseases: molecular basis of loricrin keratodermas. *Histol Histopathol* 1998; **13**: 819–826.
16 Ishida-Yamamoto A, Takahashi H, Presland RB, Dale BA, Iizuka H. Translocation of profilaggrin N-terminal domain into keratinocyte nuclei with fragmented DNA in normal human skin and loricrin keratoderma. *Lab Invest* 1998; **78**: 1245–1253.
17 Song S, Shen C, Song G *et al.* A novel c.545-546insG mutation in the loricrin gene correlates with a heterogeneous phenotype of loricrin keratoderma. *Br J Dermatol* 2008; **159**: 714–719.
18 Yoneda K, Furukawa T, Zheng YJ *et al.* An autocrine/paracrine loop linking keratin 14 aggregates to tumor necrosis factor alpha-mediated cytotoxicity in a keratinocyte model of epidermolysis bullosa simplex. *J Biol Chem* 2004; **279**: 7296–7303.
19 Inoue T, Yoneda K, Manabe M, Demitsu T. Spontaneous regression of merkel cell carcinoma: a comparative study of TUNEL index and tumor-infiltrating lymphocytes between spontaneous regression and non-regression group. *J Dermatol Sci* 2000; **24**: 203–211.
20 Yoneda K, Fujimoto T, Imamura S, Ogawa K. Distribution of fodrin in the keratinocyte *in vivo* and *in vitro*. *J Invest Dermatol* 1990; **94**: 724–729.
21 Ishida-Yamamoto A, Kato H, Kiyama H *et al.* Mutant loricrin is not crosslinked into the cornified cell envelope but is translocated into the nucleus in loricrin keratoderma. *J Invest Dermatol* 2000; **115**: 1088–1094.
22 DiColandrea T, Karashima T, Maatta A, Watt FM. Subcellular distribution of envoplakin and periplakin: insights into their role as precursors of the epidermal cornified envelope. *J Cell Biol* 2000; **151**: 573–586.
23 Boukamp P, Petrussevska RT, Breitkreutz D, Hornung J, Markham A, Fusenig NE. Normal keratinization in a spontaneously immortalized aneuploid human keratinocyte cell line. *J Cell Biol* 1988; **106**: 761–771.
24 Sitailo LA, Jerome-Morais A, Denning MF. Mcl-1 functions as major epidermal survival protein required for proper kertinocyte differentiation. *J Invest Dermatol* 2009; **129**: 1351–1360.

25 Smith FJ, Irvine AD, Terron-Kwiatkowski A *et al.* Loss-of-function mutations in the gene encoding filaggrin cause ichthyosis vulgaris. *Nat Genet* 2006; **38**: 337–342.
26 Palmer CN, Irvine AD, Terron-Kwiatkowski A *et al.* Common loss-of-function variants of the epidermal barrier protein filaggrin are a major predisposing factor for atopic dermatitis. *Nat Genet* 2006; **38**: 441–446.
27 Dale BA, Presland RB, Lewis SP, Underwood RA, Fleckman P. Transient expression of epidermal filaggrin in cultured cells causes collapse of intermediate filament networks with alteration of cell shape and nuclear integrity. *J Invest Dermatol* 1997; **108**: 179–187.
28 Kuechle MK, Presland RB, Lewis SP, Fleckman P, Dale BA. Inducible expression of filaggrin increases keratinocyte susceptibility to apoptotic cell death. *Cell Death Differ* 2000; **7**: 566–573.
29 Takahashi H, Komatsu N, Ibe M, Ishida-Yamamoto A, Hashimoto Y, Iizuka H. Cystatin A suppresses ultraviolet B-induced apoptosis of keratinocytes. *J Dermatol Sci* 2007; **46**: 179–187.
30 Presland RB, Coulombe PA, Eckert RL, Mao-Qiang M, Feingold KR, Elias PM. Barrier function in transgenic mice overexpressing K16, involucrin, and filaggrin in the suprabasal epidermis. *J Invest Dermatol* 2004; **123**: 603–606.
31 Presland RB, Kuechle MK, Lewis SP, Fleckman P, Dale BA. Regulated expression of human filaggrin in keratinocytes results in cytoskeletal disruption, loss of cell-cell adhesion, and cell cycle arrest. *Exp Cell Res* 2001; **270**: 199–213.

Physiol Genomics 40: 94–99, 2010.
First published October 27, 2009; doi:10.1152/physiolgenomics.00123.2009.

Identification and characterization of a novel *ABCA3* mutation

Sang-Kyu Park,[1,2,3]* Louella Amos,[1]* Aparna Rao,[1] Michael W. Quasney,[1,2,3] Yoshihiro Matsumura,[4] Nobuya Inagaki,[5] and Mary K. Dahmer[1,2,3]

[1]*Department of Pediatrics,* [2]*Children's Research Institute, and* [3]*Human and Molecular Genetics Center, Medical College of Wisconsin, Milwaukee, Wisconsin;* [4]*Department of Biochemistry and Molecular Biology, Oregon Health and Science University, Portland, Oregon; and* [5]*Department of Diabetes and Clinical Nutrition, Kyoto University, Kyoto, Japan*

Submitted 31 July 2009; accepted in final form 25 October 2009

Park SK, Amos L, Rao A, Quasney MW, Matsumura Y, Inagaki N, Dahmer MK. Identification and characterization of a novel *ABCA3* mutation. *Physiol Genomics* 40: 94–99, 2010. First published October 27, 2009; doi:10.1152/physiolgenomics.00123.2009.—Mutations in the gene coding for ATP-binding cassette protein A3 (ABCA3) are recognized as a genetic cause of lung disease of varying severity. Characterization of a number of mutant ABCA3 proteins has demonstrated that the mutations generally affect intracellular localization or the ability of the protein to hydrolyze ATP. A novel heterozygous mutation that results in the substitution of cysteine for arginine at amino acid 295 in ABCA3 was identified in a premature infant with chronic respiratory insufficiency and abnormal lamellar bodies. Sequencing of DNA performed in study participants demonstrated that this was a mutation and not a common variant. Plasmid vectors containing *ABCA3* with the identified novel mutation tagged with green fluorescent protein on the carboxy terminus were generated. The effect of the mutation on protein function was characterized by examining the glycosylation state of the mutant protein in transiently transfected HEK293 cells and by examining ATP hydrolysis activity of the mutant protein with a vanadate-induced nucleotide trapping assay in stably transfected HEK293 cells. The ABCA3 protein containing the R295C mutation undergoes normal glycosylation and intracellular localization but has dramatically reduced ATP hydrolysis activity (12% of wild type). The identification of one copy of this novel mutation in a premature infant with chronic respiratory insufficiency suggests that *ABCA3* haploinsufficiency together with lung prematurity may result in more severe, or more prolonged, respiratory failure.

chronic respiratory insufficiency; surfactant; pediatrics; lung disease

SURFACTANT IS ESSENTIAL for normal lung function partly by lowering alveolar surface tension and preventing end-expiratory atelectasis. Surfactant is found in lamellar bodies in type II pneumocytes and is composed of phospholipids and the surfactant-associated proteins SP-A, SP-B, SP-C, and SP-D. Inherited mutations in SP-B and SP-C are associated with respiratory failure (6, 10, 18). Loss-of-function mutations on both alleles of SP-B result in surfactant deficiency, severe neonatal lung disease, and in some instances death. SP-C deficiency is generally less severe, resulting in a spectrum of respiratory problems, ranging from neonatal disease to childhood interstitial lung disease.

Recently, mutations in the ATP-binding cassette protein A3 (ABCA3) gene have been recognized as another cause of surfactant deficiency and lung disease (1, 2, 10, 20). ABCA3 is a member of the ABC family of transmembrane proteins involved in the transport of a variety of substrates across membranes (11). ABC proteins bind and hydrolyze ATP, and hydrolysis of ATP is required for the protein to function as a transporter. ABCA3 is specifically found in the limiting membrane of surfactant-storing intracellular lamellar bodies in type II alveolar epithelial cells (16, 21). Recent evidence indicates that ABCA3 transports lipids essential for surfactant synthesis and function into lamellar bodies (5, 8, 15, 17).

Mutations in *ABCA3* have been found to cause lung disease of varying severity. Over 70 *ABCA3* mutations have been identified in full-term infants with respiratory failure and children with interstitial lung disease (10), although the functional impact of many of these mutants has not been explored. Little is known about the effect of *ABCA3* mutations on premature infants who are predisposed to chronic lung disease because of their prematurity, although there is one report suggesting that a single nucleotide polymorphism (SNP) in *ABCA3* may be associated with a prolonged course of respiratory distress syndrome (RDS) in very premature infants (12).

In the present study, we have identified a novel mutation in the gene coding for ABCA3 in a premature Hmong infant with chronic respiratory insufficiency. This mutation substitutes a cysteine for an arginine at amino acid position 295 in the first intracellular loop (ICL-1) of ABCA3. Functional analysis of this R295C mutation demonstrates that the mutation severely compromises the ability of the protein to hydrolyze ATP.

MATERIALS AND METHODS

Enrollment of subjects. Individuals of a Hmong community in Wisconsin eligible for enrollment included *1*) healthy unrelated adults ≥18 yr of age of Hmong descent on no medications or *2*) parents and relatives of the index case. Subjects were identified through community outreach and the parents of the index case. Subjects who could not speak English were excluded, as were individuals whose immediate family member or first-degree relative was already enrolled. Research personnel obtained written consent from eligible subjects, and a buccal swab was obtained. A unique code was applied to the swab, and no identifiers were obtained by the investigators, with the exception of the parents and relatives of the index case. This study was approved by the Institutional Review Board.

DNA analysis. Buccal swabs were stored at −20°C until extraction. DNA was extracted from buccal swabs with the Epicentre MasterAmp Buccal Swab DNA Extraction kit (MB79015) and stored at −80°C.

DNA samples were amplified in the region of the variant with AmpliTaq Gold polymerase (Applied Biosystems, Foster City, CA) and the primers 5′-TCACCTTGACACAGAAGAGCAG-3′ and 5′-AGTAAGACCCTGTCGAATGCAG-3′. The PCR reaction conditions were 96°C for 5 min followed by 40 cycles of 94°C for 30 s, 55°C for 30 s, 72°C for 45 s, followed by 72°C for 10 min. The PCR product (248 bp) was treated with ExoSAP-IT (USB, Cleveland, OH) and sequenced.

* S.-K. Park and L. Amos contributed equally to the project and authorship of the manuscript.

Address for reprint requests and other correspondence: M. K. Dahmer, Div. of Critical Care, Dept. of Pediatrics, Medical College of Wisconsin, 9000 West Wisconsin Ave., MS681, Milwaukee, WI 53201 (e-mail: mdahmer@mcw.edu).

Cell culture. HEK293 cells purchased from American Type Culture Collection (Manassas, VA) were maintained in Dulbecco's modified Eagle's medium (DMEM; Invitrogen, Carlsbad, CA) supplemented with penicillin (100 U/ml), streptomycin (100 μg/ml), 25 mM HEPES, and 10% fetal bovine serum (FBS) in a humidified atmosphere of 5% CO_2 at 37°C.

DNA construction. The R295C mutant was initially generated from the pEGFPN1-ABCA3-green fluorescent protein (GFP) construct (14) with the QuikChange II XL site-directed mutagenesis kit (Stratagene, La Jolla, CA) and the following primers: forward 5′-AGGCTGAAGGAGTACATGTGCATGATGGGGCTCAGCAG-3′ and reverse 5′-CTGCTGAGCCCCATCATGCACATGTACTCCTTCAGCCT-3′ (underlines indicate substituted nucleotides). A R295C-GFP construct in a pCAGIpuro vector was generated by inserting the coding region of ABCA3-R295C-GFP into the pCAGIpuro vector. Presence of the mutation in the pEGFN1-ABCA3-R295C-GFP and pCAGIpuro-ABCA3-R295C-GFP constructs was confirmed by sequencing.

Glycosylation of wild-type and mutant ABCA3-GFP proteins. Transient transfections of HEK293 cells with wild-type *ABCA3*-GFP and *ABCA3* mutants L101P-GFP, N568D-GFP, and L982P-GFP (14), as well as the new pEGFPN1 construct for R295C-GFP, were performed with FuGENE 6 transfection reagent (Roche Applied Science, Indianapolis, IN) as previously described (14). Briefly, for each experiment cells were seeded into 100-mm dishes at a density of 3×10^6/dish for the assay and cultured for 1 day, and each plate was then transfected with 6 μg of one of the plasmid vectors listed above. Cells were cultured for an additional 48 h and lysed, and membranes were prepared as described previously (14). Membrane protein (10 μg) was treated with 100 U of peptide N-glycosidase F (PNGase F) or 500 U of endoglycosidase H (Endo H) (New England Biolabs, Beverly, MA) for 30 min at 37°C in a total volume of 20 μl. The samples were then electrophoresed on 5% SDS-polyacrylamide gels, and immunoblot analysis was performed with anti-GFP monoclonal antibody (Santa Cruz Biotechnology, Santa Cruz, CA).

Stable transfection of wild-type and mutant ABCA3-GFP. Clonally selected HEK293 cell lines stably expressing wild-type or various mutant *ABCA3*-GFP genes were developed as previously described (14) and maintained in DMEM containing 2.5 μg/ml puromycin (Sigma, St. Louis, MO).

Vanadate-induced nucleotide trapping assay of wild-type and mutant ABCA3-GFP proteins. Vanadate-induced nucleotide trapping was performed with 8-azido-[α-^{32}P]ATP purchased from Affinity Labeling Technologies (ALT, Lexington, KY) as described previously (14). Samples were analyzed by SDS-PAGE on 5% polyacrylamide gel, electrotransferred onto nitrocellulose membranes (Bio-Rad, Hercules, CA), and quantified with a STORM 860 PhosphorImager system (Amersham Biosciences, Piscataway, NJ). Each experiment was performed on a different passage of stably transfected cell lines.

RESULTS

Identification of a novel R295C mutation. A Hmong male born at 25 wk of gestation (weighing 790 g) was intubated at birth and received surfactant therapy for RDS. He required high-frequency oscillatory ventilation for 2½ mo and conventional mechanical ventilation for 1 mo and was eventually transitioned to noninvasive ventilation. After a 4-mo hospitalization in the neonatal intensive care unit, he was discharged on oxygen therapy with a nasal cannula. Within 4 wk of discharge, he was hospitalized with worsening respiratory failure, increasing oxygen need, and poor weight gain. Chest computerized tomography demonstrated coarse interstitial opacities, cystic changes, and focal hyperinflation, while bronchoscopy revealed normal upper and lower airway anatomy. Despite appropriate medical therapies, the child was hospital-

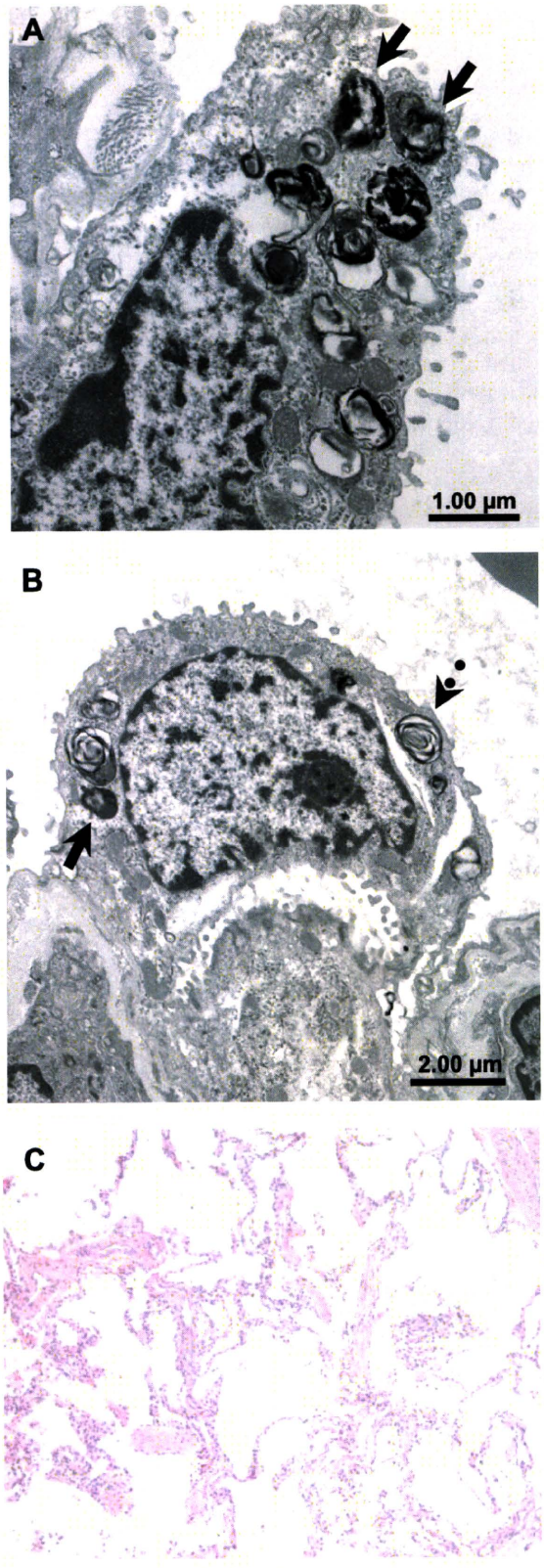

Fig. 1. Microscopy of the lung biopsy from a patient with chronic respiratory insufficiency. *A* and *B*: electron microscopy demonstrating abnormal lamellar bodies (solid arrows) and normal lamellar bodies (dashed arrows). Some cells have a combination of normal and abnormal lamellar bodies. *C*: hematoxylin and eosin staining (magnification ×20) demonstrating irregular dilatation and reduced number of peripheral alveoli with thickened smooth muscle in arterial walls.

ized during the majority of his first year of life for refractory respiratory insufficiency and eventually had a tracheostomy at age 1 yr. To determine whether the chronic respiratory insufficiency observed might be due to an inherited disorder resulting in surfactant deficiency, genetic testing (for mutations in the genes for SP-B, SP-C, and ABCA3 by sequencing of exons and splice sites) and a lung biopsy were performed. Lung biopsy demonstrated the presence of abnormal lamellar bodies (Fig. 1; some normal lamellar bodies were also observed) and chronic bronchopulmonary dysplasia (BPD) with persistent fetal pulmonary architecture. DNA sequencing revealed no mutations in the genes coding for SP-B and SP-C; however, the child was heterozygous for a novel variation in the *ABCA3* gene (replacement of a C with a T at nucleotide position 883). This change results in the replacement of arginine by cysteine at amino acid position 295. No other mutations in *ABCA3* were identified.

Although the R295C variant had not been observed in previously characterized populations, it was unclear whether the R295C variant was a common polymorphism in Hmong individuals or a clinically significant mutation. To determine whether the R295C variant was a polymorphism or a mutation, the frequency of this variant in the Hmong population was examined. DNA from individuals from the child's family, and from individuals in the Hmong community, was sequenced in the region of the variation. DNA samples from 90 of 91 individuals from the general Hmong population were sequenced successfully. None of these individuals had the R295C variant, indicating that this variation is indeed a mutation and not a polymorphism. Several members of the child's immediate family, including one of the parents, were heterozygous for the mutation.

Effects of ABCA3 R295C mutation on function. The R295C mutation is located in the first ICL (ICL-1) of the protein (Fig. 2*A*) and is adjacent to the previously reported mutant E292V (2). The R295C mutation resides in a region that is conserved in different members of the ABCA subfamily (Fig. 2*B*) and across ABCA3 homologs in vertebrates (Fig. 2*C*). Previous studies (4, 13, 14) have identified mutations that affect ABCA3 function by either altering intracellular localization (type I mutants) or impairing ATP hydrolysis activity (type II mutants).

To examine whether the intracellular localization of the R295C mutant was altered, the glycosylation state of the R295C mutant was characterized. Membranes from HEK293 cells expressing wild-type *ABCA3*-GFP, the R295C-GFP mutant, or several previously characterized mutants were examined for sensitivity to the glycosidases Endo H and PNGase F. In HEK293 cells, wild-type ABCA3-GFP is mainly localized in lysosomal organelles, mimicking the trafficking of ABCA3 to lamellar bodies in alveolar type II cells (14). Because Endo H only cleaves sugars from high-mannose oligosaccharides, and not from complex oligosaccharides, resistance to Endo H indicates that the protein is in post-Golgi membranes (presumably lamellar body-like organelles). After treatment

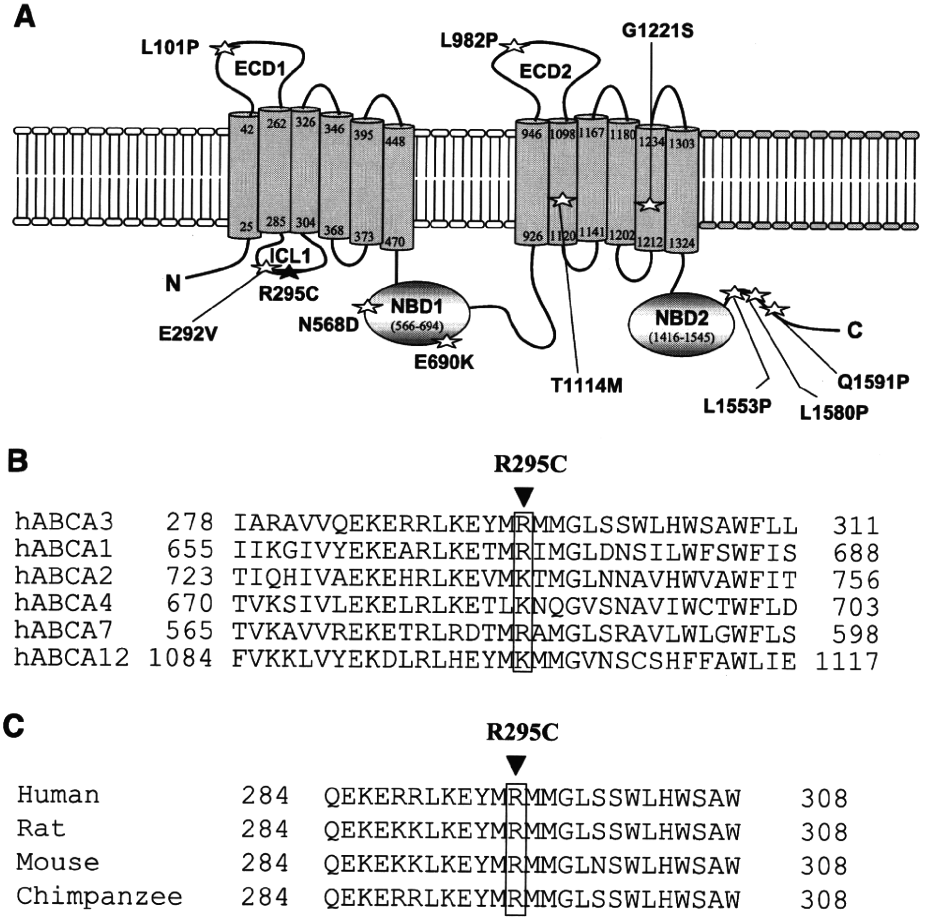

Fig. 2. Schematic diagram of ATP-binding cassette protein A3 (ABCA3) and conservation of amino acids in the region of the R295C mutant. *A*: schematic diagram of the ABCA3 protein. ☆, Mutations reported previously; ★, novel mutant R295C. ECD1 and ECD2, extracellular domains; ICL-1, intracellular loop 1; NBD1 and NBD2, nucleotide binding domains. Type I mutations include L101P, L982P, L1553P, and Q1591P; type II mutations include E292V, N568D, E690K, T1114, G1221S, and L1580P (13, 14). *B*: alignment of sequences surrounding the R295C mutation in ICL-1 in various members of the ABCA subfamily. *C*: alignment of sequences surrounding the R295C mutation in human, rat, mouse, and chimpanzee.

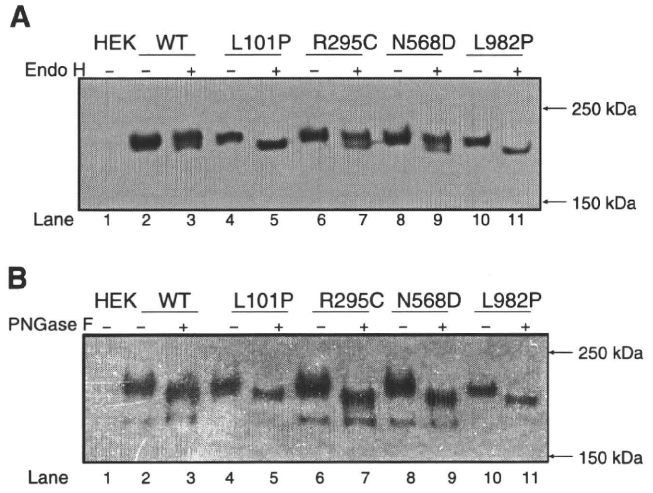

Fig. 3. Glycosylation of wild-type (WT) and mutant ABCA3-green fluorescent protein (GFP) proteins. *A*: 20 μg of membrane fraction from HEK293 cells transiently transfected with WT ABCA3-GFP (*lanes 2* and *3*) or with ABCA3-GFP mutants L101P (*lanes 4* and *5*), R295C (*lanes 6* and *7*), N568D (*lanes 8* and *9*), and L982P (*lanes 10* and *11*) were treated without (−) or with (+) endoglycosidase H (Endo H) and analyzed by 5% SDS-PAGE followed by immunoblotting with anti-GFP antibody. *Lane 1*, immunoblotting of untransfected HEK293 cells. *B*: WT ABCA3-GFP (*lanes 2* and *3*) or ABCA3-GFP mutants L101P (*lanes 4* and *5*), R295C (*lanes 6* and *7*), N568D (*lanes 8* and *9*), and L982P (*lanes 10* and *11*) were treated without (−) or with (+) peptide N-glycosidase F (PNGase F) and were then analyzed by 5% SDS-PAGE followed by immunoblotting with anti-GFP antibody. *Lane 1*, immunoblotting of untransfected HEK293 cells. Results from 1 representative experiment from a total of 3 separate experiments are shown.

with Endo H the wild-type ABCA3 protein is present as a doublet (Fig. 3*A*, *lane 3*), with much of the protein being resistant to Endo H, suggesting it is in post-Golgi membranes (Fig. 3*A*, compare *lanes 2* and *3*). This observation is consistent with previous reports. The R295C variant demonstrated a level of resistance to Endo H comparable to that of the wild-type protein (Fig. 3*A*, compare *lanes 6* and *7* to *lanes 2* and *3*), suggesting that the variant protein has undergone normal glycosylation and resides in post-Golgi membranes. As reported previously, the N568D variant shows resistance to Endo H (Fig. 3*A*, *lanes 8* and *9*) at a level similar to that of the wild-type protein; however, the L101P and L982P variants (Fig. 3*A*, *lanes 4* and *5* and *lanes 10* and *11*, respectively) show no Endo H resistance, indicating that these mutants have not left the endoplasmic reticulum (14). As expected, the wild-type and mutant ABCA3 proteins are all sensitive to PNGase F (Fig. 3*B*), which cleaves both high-mannose and complex oligosaccharide from N-linked glycoproteins.

To determine whether the R295C mutation affected the ATP hydrolysis activity of the R295C mutant, vanadate-induced nucleotide trapping with photoaffinity labeling of the trapped intermediate (3) was examined. In this assay, ATP hydrolysis with production of a stable intermediate can be assessed based on the intensity of photoaffinity labeling of the ABCA3 protein. As shown in Fig. 4*A*, the level of vanadate-induced nucleotide trapping in the R295C mutant was greatly reduced compared with that of the wild-type ABCA3 protein. The level of the ABCA3-R295C-GFP mutant protein was comparable to that of wild-type ABCA3-GFP as demonstrated in the anti-GFP immunoblot. Vanadate-induced nucleotide trapping was also decreased in the N568D mutant as reported previously (14). Quantitation of three independent experiments demonstrated that the degree of trapping in the R295C mutant was dramatically reduced to 12% of that of the wild type (Fig. 4*B*). These results indicate that the ability of the R295C mutant to hydrolyze ATP is severely impaired.

DISCUSSION

The results presented here demonstrate that R295C is a novel mutation that results in severely impaired ATP hydrolysis activity as indicated by the dramatic reduction in vanadate-induced nucleotide trapping. Other mutations in the ABCA3 protein also result in impaired ATP hydrolysis, including E292V, N568D, G1221S, L1580P, and T1114M (13, 14). The E292V mutation is in ICL-1 only three amino acids from the R295C mutation. Clearly, the presence of two mutations that affect ATP hydrolysis in this ICL suggests that the ICL is important for normal ATP hydrolysis activity and normal

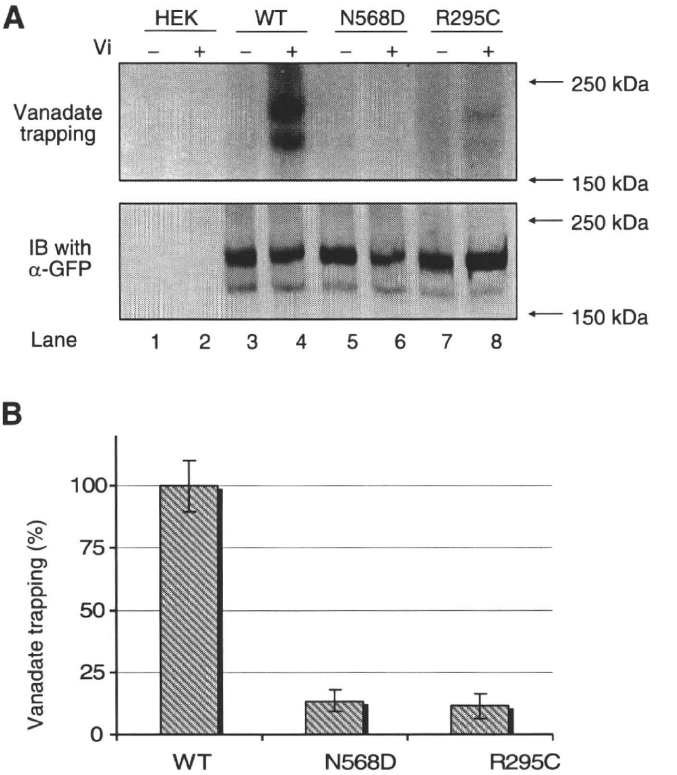

Fig. 4. Vanadate-induced nucleotide trapping in ABCA3-GFP and ABCA3-GFP mutants. *A*: 20 μg of membrane fraction from untransfected HEK293 cells (*lanes 1* and *2*), HEK293 cells stably expressing WT ABCA3-GFP (*lanes 3* and *4*), ABCA3-GFP mutants N568D (*lanes 5* and *6*), and R295C (*lanes 7* and *8*) were incubated with 20 μM 8-azido-[α-^{32}P]ATP in the absence (−) or presence (+) of 0.4 mM orthovanadate (Vi) and 3 mM $MgCl_2$ as described under MATERIALS AND METHODS. Photoaffinity-labeled ATP was detected by autoradiography (*top*) and immunoblotting (IB) using anti-GFP antibody (α-GFP) was used as a loading control (*bottom*). Results from 1 representative experiment from 3 separate experiments performed are shown. *B*: radioactivity of photoaffinity-labeled protein bands was measured and quantified (220 kDa of upper band intensities + 220 kDa of lower band intensities) with STORM 860 PhosphorImager. These were normalized to ABCA3-GFP protein from immunoblot (220 kDa of upper band intensities + 220 kDa of lower band intensities), and then radioactivity in the absence of orthovanadate was subtracted from that in the presence of orthovanadate. Data shown are means ± SD for 3 separate experiments (n = 3), 1 of which is shown in *A*.

functioning of the protein. This conclusion is also supported by the crystal structure of the bacterial ABC protein SAV1866, which suggests that ICLs transmit conformational changes important for function of the protein (7), and by the report of a mutation that reduces ATP hydrolysis activity in an ICL of multidrug resistance protein 1, another human ABC transporter protein (19).

The R295C mutation does not affect glycosylation and intracellular localization of the protein. The trafficking of proteins accompanies the processing of oligosaccharides from high-mannose to complex sugar types, with the presence of complex oligosaccharides indicating that the protein is in post-Golgi membranes. Resistance to Endo H has been demonstrated previously to be associated with localization of the ABCA3 protein to lamellar body-like organelles (14). Normal glycosylation and intracellular localization of the R295C mutant is indicated by the similar levels of sensitivity to Endo H and PNGase F observed for the wild-type ABCA3-GFP protein and the R295C mutant. The observation that a substantial portion of the R295C mutant protein is resistant to Endo H indicates that the mutation does not affect intracellular localization.

Although it is clear that the mutation impairs the function of the ABCA3 protein, the patient in whom this mutation was discovered is heterozygous for the mutation. While it is possible that either a mutation in a regulatory region of the noncoding sequence or an insertion or deletion of one or more exons might be present in the second copy of the *ABCA3* gene, it is more likely that the child has one normal copy of the *ABCA3* gene and consequently has normal as well as impaired ABCA3 protein. That the mutation has an effect on the cellular level of functional ABCA3 is indicated by the abnormal lamellar bodies observed in the patient's alveolar epithelial cells, although normal lamellar bodies are also present. Because one of the child's parents and two siblings also have the mutation and none has a history of severe lung disease, it is likely that there is sufficient functional ABCA3 present for normal lung function under normal conditions. However, the patient was born prematurely and was exposed to a number of stresses that are not seen in term infants, consequently haploinsufficiency (having just 1 functional copy of the gene) may explain the more severe injury and/or prolonged recovery period observed in this patient. Most premature infants require only supplemental oxygen on discharge from the neonatal intensive care unit; rarely do they need tracheostomy for long-term mechanical ventilation as was required for this patient. (By 2.5 yr old this patient had improved enough that a tracheostomy was no longer required.) This patient's haploinsufficiency may have caused surfactant dysfunction milder than would be expected in an individual homozygous for the mutation, but significant enough to cause chronic respiratory insufficiency in a premature infant. One possibility is that an interaction between the R295C mutation and the patient's prematurity resulted in the severe BPD observed. As has been suggested for individuals heterozygous for functional SP-B mutations (10), it is possible that for children heterozygous for a functional *ABCA3* mutation any environmental or developmental stress that alters *ABCA3* expression may result in more severe respiratory stress because of their already reduced level of functional ABCA3. Interestingly, the frequency of individuals heterozygous for the E292V mutation is elevated in a cohort of children with RDS, suggesting that a mutation in this region might impart increased genetic risk for respiratory insufficiency, even in heterozygotes (9).

In conclusion, clinical management of a premature infant with severe BPD and chronic respiratory failure led to the discovery of the novel *ABCA3* mutation R295C. This mutation, present in ICL-1, does not affect intracellular localization but severely impairs ATP hydrolysis activity of the ABCA3 mutant protein and is likely responsible for the aberrant lamellar bodies observed on lung biopsy. The identification of one copy of this novel mutation in a premature infant with chronic respiratory insufficiency suggests that *ABCA3* haploinsufficiency together with lung prematurity may result in more severe, or more prolonged, respiratory failure. Testing for *ABCA3* mutations in infants with refractory respiratory insufficiency or respiratory failure and a history of prematurity may help identify new mutations, clarify the function of ABCA3 and its various domains, and explain observed clinical deterioration despite appropriate medical management.

ACKNOWLEDGMENTS

We thank Daniel Merchant for excellent technical assistance and Dr. James F. Southern for providing histological analysis.

GRANTS

This work was supported, in part, by the Children's Research Institute at the Medical College of Wisconsin.

DISCLOSURES

No conflicts of interest are declared by the author(s).

REFERENCES

1. **Brasch F, Schimanski S, Muhlfeld C, Barlage S, Langmann T, Aslanidis C, Boettcher A, Dada A, Schroten H, Mildenberger E, Prueter E, Ballmann M, Ochs M, Johnen G, Griese M, Schmitz G.** Alteration of the pulmonary surfactant system in full-term infants with hereditary ABCA3 deficiency. *Am J Respir Crit Care Med* 174: 571–580, 2006.
2. **Bullard JE, Wert SE, Whitsett JA, Dean M, Nogee LM.** ABCA3 mutations associated with pediatric interstitial lung disease. *Am J Respir Crit Care Med* 172: 1026–1031, 2005.
3. **Carrier I, Julien M, Gros P.** Analysis of catalytic carboxylate mutants E552Q and E1197Q suggests asymmetric ATP hydrolysis by the two nucleotide-binding domains of P-glycoprotein. *Biochemistry* 42: 12875–12885, 2003.
4. **Cheong N, Madesh M, Gonzales LW, Zhao M, Yu K, Ballard PL, Shuman H.** Functional and trafficking defects in ATP binding cassette A3 mutants associated with respiratory distress syndrome. *J Biol Chem* 281: 9791–9800, 2006.
5. **Cheong N, Zhang H, Madesh M, Zhao M, Yu K, Dodia C, Fisher AB, Savani RC, Shuman H.** ABCA3 is critical for lamellar body biogenesis in vivo. *J Biol Chem* 282: 23811–23817, 2007.
6. **Cole FS, Nogee LM, Hamvas A.** Defects in surfactant synthesis: clinical implications. *Pediatr Clin North Am* 53: 911–917, 2006.
7. **Dawson RJ, Locher KP.** Structure of a bacterial multidrug ABC transporter. *Nature* 443: 180–185, 2006.
8. **Garmany TH, Moxley MA, White FV, Dean M, Hull WM, Whitsett JA, Nogee LM, Hamvas A.** Surfactant composition and function in patients with ABCA3 mutations. *Pediatr Res* 59: 801–805, 2006.
9. **Garmany TH, Wambach JA, Heins HB, Watkins-Torry JM, Wegner DJ, Bennet K, An P, Land G, Saugstad OD, Henderson H, Nogee LM, Cole FS, Hamvas A.** Population and disease-based prevalence of the common mutations associated with surfactant deficiency. *Pediatr Res* 63: 645–649, 2008.

10. **Hamvas A, Cole FS, Nogee LM.** Genetic disorders of surfactant proteins. *Neonatology* 91: 311–317, 2007.
11. **Kaminski WE, Piehler A, Wenzel JJ.** ABC A-subfamily transporters: structure, function and disease. *Biochim Biophys Acta* 1762: 510–524, 2006.
12. **Karjalainen MK, Haataja R, Hallman M.** Haplotype analysis of ABCA3: association with respiratory distress in very premature infants. *Ann Med* 40: 56–65, 2008.
13. **Matsumura Y, Ban N, Inagaki N.** Aberrant catalytic cycle and impaired lipid transport into intracellular vesicles in ABCA3 mutants associated with nonfatal pediatric interstitial lung disease. *Am J Physiol Lung Cell Mol Physiol* 295: L698–L707, 2008.
14. **Matsumura Y, Ban N, Ueda K, Inagaki N.** Characterization and classification of ATP-binding cassette transporter ABCA3 mutants in fatal surfactant deficiency. *J Biol Chem* 281: 34503–34514, 2006.
15. **Matsumura Y, Sakai H, Sasaki M, Ban N, Inagaki N.** ABCA3-mediated choline-phospholipids uptake into intracellular vesicles in A549 cells. *FEBS Lett* 581: 3139–3144, 2007.
16. **Mulugeta S, Gray JM, Notarfrancesco KL, Gonzales LW, Koval M, Feinstein SI, Ballard PL, Fisher AB, Shuman H.** Identification of LBM180, a lamellar body limiting membrane protein of alveolar type II cells, as the ABC transporter protein ABCA3. *J Biol Chem* 277: 22147–22155, 2002.
17. **Nagata K, Yamamoto A, Ban N, Tanaka AR, Matsuo M, Kioka N, Inagaki N, Ueda K.** Human ABCA3, a product of a responsible gene for ABCA3 for fatal surfactant deficiency in newborns, exhibits unique ATP hydrolysis activity and generates intracellular multilamellar vesicles. *Biochem Biophys Res Commun* 324: 262–268, 2004.
18. **Nogee LM.** Alterations in SP-B and SP-C expression in neonatal lung disease. *Annu Rev Physiol* 66: 601–623, 2004.
19. **Ren XQ, Furukawa T, Yamamoto M, Aoki S, Kobayashi M, Nakagawa M, Akiyama S.** A functional role of intracellular loops of human multidrug resistance protein 1. *J Biochem (Tokyo)* 140: 313–318, 2006.
20. **Shulenin S, Nogee LM, Annilo T, Wert SE, Whitsett JA, Dean M.** ABCA3 gene mutations in newborns with fatal surfactant deficiency. *N Engl J Med* 350: 1296–1303, 2004.
21. **Yamano G, Funahashi H, Kawanami O, Zhao LX, Ban N, Uchida Y, Morohoshi T, Ogawa J, Shioda S, Inagaki N.** ABCA3 is a lamellar body membrane protein in human lung alveolar type II cells. *FEBS Lett* 508: 221–225, 2001.

Biochemical and Biophysical Research Communications 393 (2010) 73–78

Contents lists available at ScienceDirect

Biochemical and Biophysical Research Communications

journal homepage: www.elsevier.com/locate/ybbrc

Overexpression of SIRT5 confirms its involvement in deacetylation and activation of carbamoyl phosphate synthetase 1

Masahito Ogura, Yasuhiko Nakamura, Daisuke Tanaka, Xiaotong Zhuang, Yoshihito Fujita, Akio Obara, Akihiro Hamasaki, Masaya Hosokawa, Nobuya Inagaki *

Department of Diabetes and Clinical Nutrition, Graduate School of Medicine, Kyoto University, 54 Kawahara-cho, Shogoin, Sakyo-ku, Kyoto 606–8507, Japan

ARTICLE INFO

Article history:
Received 18 January 2010
Available online 25 January 2010

Keywords:
SIRT5
Mitochondria
Urea cycle
Liver

ABSTRACT

SIR2 protein, an NAD-dependent deacetylase, is localized to nucleus and is involved in life span extension by calorie restriction in yeast. In mammals, among the seven SIR2 homologues (SIRT1-7), SIRT3, 4, and 5 are localized to mitochondria. As SIRT5 mRNA levels in liver are increased by fasting, the physiological role of SIRT5 was investigated in liver of SIRT5-overexpressing transgenic (SIRT5 Tg) mice. We identified carbamoyl phosphate synthetase 1 (CPS1), a key enzyme of the urea cycle that catalyzes condensation of ammonia with bicarbonate to form carbamoyl phosphate, as a target of SIRT5 by two-dimensional electrophoresis comparing mitochondrial proteins in livers of SIRT5 Tg and wild-type mice. CPS1 protein was more deacetylated and activated in liver of SIRT5 Tg mice than in wild-type. In addition, urea production was upregulated in hepatocytes of SIRT5 Tg mice. These results agree with those of a previous study using SIRT5 knockout (KO) mice. Because ammonia generated during fasting is toxic, SIRT5 protein might play a protective role by converting ammonia to non-toxic urea through deacetylation and activation of CPS1.

Introduction

SIR2 protein is an NAD-dependent deacetylase [1]. In yeast, increasing the dosage of the SIR2 gene extends life span, whereas disruption of the SIR2 gene shortens it [2]. SIR2 determines life span not only in yeast but also in *Caenorhabditis elegans* [3] and *Drosophila melanogaster* [4]. Mammals have seven SIR2 homologues, SIRT1-7 [5]. SIRT1 deacetylates and regulates the activities of many proteins in the nucleus. SIRT1 upregulates expression of gluconeogenic genes and downregulates glycolytic genes through deacetylation of PPARγ coactivator-1α and FOXO1 [6,7].

SIRT3, SIRT4, and SIRT5 proteins are known to be localized to mitochondria [8]. *In vitro*, SIRT3 protein deacetylates and activates mitochondrial enzymes such as glutamate dehydrogenase, isocitrate dehydrogenase 2, and acetyl CoA synthetase 2 (AceCS2) [9–11]. While SIRT4 does not have NAD-dependent deacetylase activity, it does have ADP-ribosyl transferase activity. SIRT4 inhibits insulin secretion by repression of glutamate dehydrogenase activity through ADP-ribosylation [12,13]. SIRT5 protein also exhibits NAD-dependent deacetylase activity on histone H4 peptide *in vitro* [13]. Recently, Nakagawa et al. reported that SIRT5 interacts with carbamoyl phosphate synthetase 1 (CPS1), and that deacetylated CPS1 is decreased and CPS1 activity is downregulated in livers of SIRT5 knockout (KO) mice [14].

During fasting or starvation, circulating amino acids are derived mainly from catabolism of skeletal muscle, and are used in gluconeogenesis in liver to maintain blood glucose levels. The ammonia co-generated in liver from these amino acids is toxic; the urea cycle detoxifies this ammonia by converting it to non-toxic, water-soluble urea, which is readily excreted from kidney [15,16].

CPS1 is the mitochondrial protein that catalyzes the first step of the urea cycle, the condensation of ammonia with bicarbonate to form carbamoyl phosphate [15,16]. Patients with CPS1 deficiency exhibit lethally severe hyperammonemia in the neonatal period [16], which suggests a critical role for CPS1 in the urea cycle.

In the present study, to investigate the physiological role of SIRT5, we generated SIRT5-overexpressing transgenic (SIRT5 Tg) mice and attempted to identify the target protein of SIRT5 regulation in liver. We show here that SIRT5 protein might regulate urea production by deacetylation and activation of mitochondrial CPS1, complementing the previous study of SIRT5 KO mice [14].

Materials and methods

Animal Experiments: The mice were housed in an air-controlled (temperature 25 °C) room with dark–light cycle (10 h; 14 h).

Abbreviations: SIR2, silent information regulator 2; CPS1, carbamoyl phosphate synthetase 1; Tg, transgenic; KO, knockout.

* Corresponding author. Fax: +81 75 771 6601.
E-mail address: inagaki@metab.kuhp.kyoto-u.ac.jp (N. Inagaki).

0006-291X/$ - see front matter © 2010 Elsevier Inc. All rights reserved.
doi:10.1016/j.bbrc.2010.01.081

Animal care and procedures were approved by the Animal Care Committee of Kyoto University.

Isolation of total RNA and quantitative RT-PCR: Total RNA was isolated from livers, kidneys and hearts of 11 week-old C57BL/6 mice using Trizol (Invitrogen), and cDNA was prepared by reverse transcriptase (Superscript II; Invitrogen) with an oligo (dT) primer. SIRT5 mRNA levels were measured by real-time quantitative RT-PCR using ABI PRISM 7000 Sequence Detection System (Applied Biosystems). SIRT5 mRNA levels were corrected for β-actin mRNA levels. The mouse sequences of forward and reverse primers to evaluate SIRT5 expression were 5′-GTCATCACCCAGAACATCGA-3′ and 5′-ACGTGAGGTCGCAGCAAGCC-3′; respectively. The mouse sequences of forward and reverse primers to evaluate β-actin expression were 5′-TTGCAGCTCCTTCGTTGC-3′ and 5′-CACGAT GGAGGGGAATACAG-3′, respectively. SYBR Green PCR Master Mix (Applied Biosystems) was prepared for PCR run. The thermal cycling conditions were denaturation at 95 °C for 10 min followed by 50 cycles at 95 °C for 15 s and 60 °C for 1 min.

Plasmid construction: The expression vectors for SIRT5 protein with (pCMV5aSIRT5-FLAG) and without (pCMV5aSIRT5) FLAG tag at the C-terminus were constructed as follows. The coding region of mouse SIRT5 cDNA was cloned by PCR using mouse liver cDNA prepared as described above. The PCR fragments were subcloned into pFLAG-CMV-5a (Sigma).

Antibody: SIRT5 polyclonal antibody was produced by immunizing a rabbit with synthetic peptide CGKTLPEALAPHETE, corresponding to 15 C-terminal amino acid residues of mouse SIRT5 protein. The antibody was purified by HiTrap NHS-activated HP kit (GE Healthcare) and gel filtration column. Western blotting analysis was performed using the obtained anti-SIRT5 or anti-FLAG (Sigma) antibodies.

Generation of SIRT5-overexpressing transgenic mice: SIRT5 cDNA with FLAG tag sequences was inserted to the *Eco*RI site of transgenic plasmid pIns-1 [17], and the human insulin promoter of pIns-1 was then replaced by the CAG promoter derived from pCAGGS plasmid [18]. The transgene cassettes were excised from the resulting plasmid by digestion with *Not*I and *Xho*I, and the linearized cassettes were microinjected to fertilized eggs of C57BL/6 inbred mice (PhoenixBio CO., Ltd. Hiroshima, Japan). Since the two lines revealed similar data, all additional experiments were performed using line #38.

Preparation of mitochondria: The livers of C57BL/6 mice were homogenized in isotonic buffer (PBS containing 0.25 M sucrose) containing protease inhibitors (Complete, EDTA free: Roche) with potter homogenizer. The mitochondria were prepared as described previously [8].

Two-dimensional electrophoresis and identification of protein: Liver mitochondria were prepared as described previously [8] and lysed with rehydration buffer (8 M urea, 2% CHAPS, 50 mM DTT, 0.2% Bio-Lyte (BIO-RAD), 0.001% bromophenol blue), and applied to ReadyStrip IPG Strip (BIO-RAD) and separated by isoelectric focusing electrophoresis with a range pH 5 to pH 8 using PROTEAN IEF cell (BIO-RAD). The IPG Strip was then subjected to SDS–polyacrylamide gel electrophoresis. The obtained gel was stained with SYPRO Ruby protein gel stain kit (invitrogen), and the protein was visualized and analyzed using Typhoon 9210 (GE healthcare). The protein at the indicated spot was isolated and analyzed using MALDI-TOF-MS (APRO Life Science Institute, Inc.).

Immunoprecipitation: Mitochondria lysed with PBS containing 1% Triton X-100 were incubated with anti-CPS1 (Santa Cruz) or anti-acetylated lysine (Cell Signaling) antibody for 16 h at 4 °C. Protein G Sepharose (GE healthcare) was then added and incubation was continued for 3 h. The resin was washed and boiled with SDS sample buffer (0.2 M Tris, 10% sucrose, 10% SDS, 5 mM EDTA). The sample was analyzed by western blotting with anti-CPS1 antibody.

Determination of CPS1 activity: Livers of 8–12 week-old SIRT5 Tg and wild-type mice fasted for 16 h were homogenized [19] and CPS1 activities were assayed as described by Fahien and Cohen [20]. Briefly, the reaction was started by adding the supernatant obtained above (enzyme source) to the assay mixture containing 2.5 mM phosphoenopyruvate, 0.2 mM NADH, 10 mM NH_4Cl, 100 mM $KHCO_3$, 5 mM ATP, 10 mM $MgSO_4$, 10 mM *N*-acetylglutamate, 10 U/ml pyruvate kinase (SIGMA), 12.5 U/ml of lactate dehydrogenase (SIGMA), and 50 mM glycylglycine (pH 7.6) at room temperature, and the decrease in absorbance at 340 nm was measured. The initial velocity of the reaction was directly proportional CPS1 activity. One unit of CPS1 activity corresponded to oxidation of 1 μmol of NADH/min at room temperature.

Measurement of hepatic urea production: Hepatocytes of 8–12 week-old SIRT5 Tg and wild-type mice fasted for 16 h were isolated as described previously [21]. Obtained hepatocytes (1.5×10^5) were incubated at 37 °C in humidified atmosphere (5% CO_2) in 2 ml Krebs ringer buffer with 25 mM $NaHCO_3$, 10 mM NH_4Cl, and 5 mM ornithin–HCl [22]. Incubation was stopped by placing the cells on ice, followed by centrifugation at 4 °C for 10 min at 600*g*. The supernatant was removed and urea concentration was measured by diacetyl monoxime methods [23,24], the cells were lysed with 0.1% SDS, and the protein concentration was determined (Bio-Rad Protein Assay Kit).

Statistical analysis: Values are expressed as means ± SEM. Statistical analysis was performed unpaired Student's *t*-test. *P* values <0.05 were considered significant.

Results

Upregulation of SIRT5 mRNA levels by fasting

Expression levels of SIRT1 mRNA are known to be increased in liver and heart by fasting [25]. However, it is unclear whether the expression levels of SIRT5 are regulated by nutrient conditions. To evaluate alteration of SIRT5 mRNA expression levels in different nutrient conditions, total RNA was extracted from organs including liver, kidney, and heart in C57BL/6 mice fed *ad libitum*, fasted for 24 h, or refed for 24 h after 24-h fasting, and quantitative RT-PCR was carried out. SIRT5 mRNA levels in liver were increased 2.4-fold by fasting ($N = 4$, $P < 0.01$) and were decreased to fed condition levels by refeeding ($N = 4$, $P < 0.05$), but were unchanged in kidney or heart (Fig. 1), suggesting an important role of SIRT5 in liver.

Generation of SIRT5 Tg mice

To clarify the function of SIRT5 *in vivo*, we generated SIRT5-overexpressing transgenic (SIRT5 Tg) mice in which expression of mouse SIRT5 fused with FLAG tag at the C-terminus was driven by the CAG promoter (Fig. 2A). Southern blot analysis was performed for genotyping (Fig. 2B), and two independent SIRT5 Tg mouse lines were established on the C57BL/6 inbred background (Fig. 2C). One of these, mouse line #36, was generated with a low copy number of transgene; the other, mouse line #38, was generated with a high copy number of transgene. SIRT5 Tg mice showed no gross anatomical or reproductive defects. In addition, no histological abnormality was observed by light microscopic analysis in all of the organs examined. To investigate the expression of SIRT5 protein, an antibody specific for mouse SIRT5 was raised in a rabbit against a synthetic peptide corresponding to 15 C-terminal amino acid residues (CGKTLPEALAPHETE) of mouse SIRT5, which shows no similarity to other members of the SIRT family. To ascertain specificity of the antibody, mitochondrial proteins were prepared from COS7 cells transfected with the expression plasmid encoding mouse SIRT5 protein fused with FLAG tag,

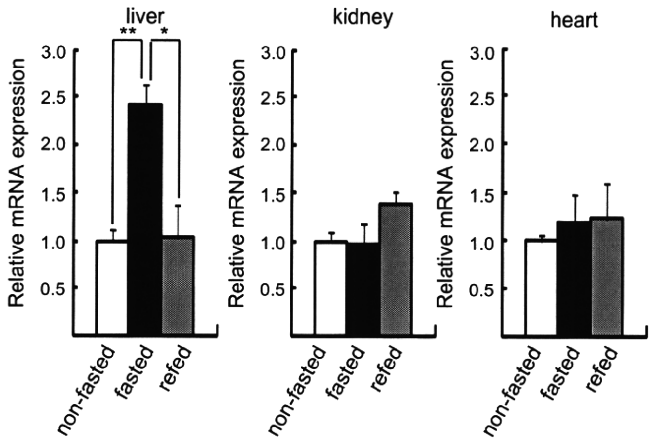

Fig. 1. Alteration of expression levels of SIRT5 mRNA by fasting and refeeding. Total RNA was isolated from livers, kidneys and hearts of 11 week-old C57BL/6 mice. Mice were divided into three groups: non-fasted ($N = 4$, open bars), fasted ($N = 4$, filled bars), and refed ($N = 4$, gray bar). The non-fasted group was fed *ad libitum*, the fasted group was fasted for 24 h, and the refed group was fasted for 24 h followed by normal chow for 24 h. The expression levels of SIRT5 mRNA were estimated by quantitative RT-PCR. SIRT5 mRNA levels were corrected for β-actin mRNA levels. Values are means ± SEM. $^{*}P < 0.05$. $^{**}P < 0.01$.

and western blotting was performed using the obtained anti-SIRT5 antibody or anti-FLAG antibody. A single band at ~32 kDa corresponding to the molecular weight of SIRT5–FLAG protein was detected with each antibody (Fig. 2D), demonstrating that this antibody specifically recognizes SIRT5 protein. Western blot analysis of mitochondrial proteins prepared from livers of the two SIRT5 Tg mouse lines using the anti-SIRT5 antibody showed that both endogenous 32-kDa SIRT5 protein and a SIRT5–FLAG protein with a molecular size somewhat larger were present, and that expression of SIRT5–FLAG protein was more abundant than that of endogenous SIRT5 protein in both Tg mouse lines (Fig. 2E).

Identification of CPS1 as a target of SIRT5 protein

Since SIRT5 mRNA levels were significantly upregulated in liver by fasting, we attempted to identify the protein that is modified by SIRT5 protein in liver. We hypothesized that deacetylation of the SIRT5 target protein might be facilitated by overexpression of SIRT5 in SIRT5 Tg mice. Because NAD-dependent deacetylase converts acetylated lysine to lysine of the target protein, its isoelectric point should shift to a higher pH value. Therefore, we performed two-dimensional electrophoresis to compare mitochondrial proteins prepared from livers of SIRT5 Tg mice and wild-type littermates; the protein samples were applied for isoelectric focusing electrophoresis, and separated by SDS–PAGE followed by staining with SYPRO Ruby. One of the proteins that newly appeared in SIRT5 Tg liver (Fig. 3A, indicated by arrow) was isolated, treated with trypsin, and analyzed by MALDI-TOF-MS (Fig. 3B). The sequences identified by mass spectrometry covered the N-terminal segment of carbamoyl phosphate synthetase 1 (CPS1) (Table. 1), suggesting that the protein is CPS1. CPS1 is a mitochondrial protein

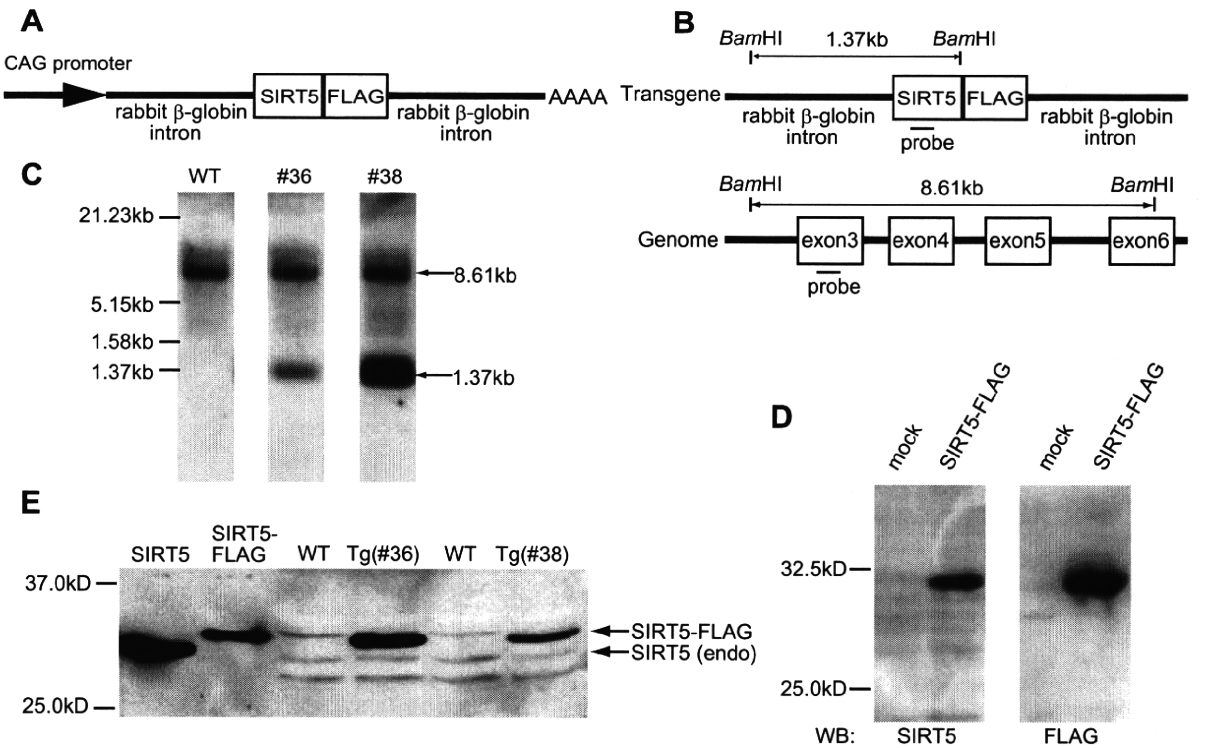

Fig. 2. Generation of SIRT5-overexpressing transgenic (SIRT5 Tg) mice and anti-SIRT5 antibody. (A) Scheme of the transgene used to generate SIRT5 Tg mice. The CAG promoter drives expression of mouse SIRT5 fused with FLAG tag at the C-terminus (SIRT5–FLAG). (B) Location of probes for Southern blot analysis. The probe corresponding to the DNA sequence in exon3 of mouse SIRT5 gene detects an 8.61-kb fragment in genomic DNA and a 1.37-kb fragment in the transgene after digestion with *Bam*HI. (C) Southern blot analysis of *Bam*HI-digested genomic DNA of wild-type (left panel) and SIRT5 Tg mice (middle panel: #36 transgenic mouse line, right panel: #38 transgenic mouse line). Southern blotting was performed with the probe indicated in (B). (D) Ascertainment of anti-SIRT5 antibody. The plasmid encoding mouse SIRT5 protein fused with FLAG tag (pCMV5aSIRT5–FLAG) was transfected to COS7 cells. Mitochondrial proteins were prepared from transfected and mock-transfected cells, and western blotting was performed with anti-SIRT5 antibody (left panel) and anti-FLAG antibody (right panel). (E) Overexpression of SIRT5–FLAG protein in SIRT5 Tg mice. Mitochondrial proteins were prepared from cells transfected with the plasmid encoding mouse SIRT5 without (pCMV5aSIRT5) or with FLAG (pCMV5aSIRT5–FLAG) and from livers of SIRT5 Tg mice and wild-type littermates (#36 and #38 transgenic mouse lines), and western blot analysis was performed using anti-SIRT5 antibody. Endogenous SIRT5 (endo) and SIRT5–FLAG proteins are indicated by arrows.

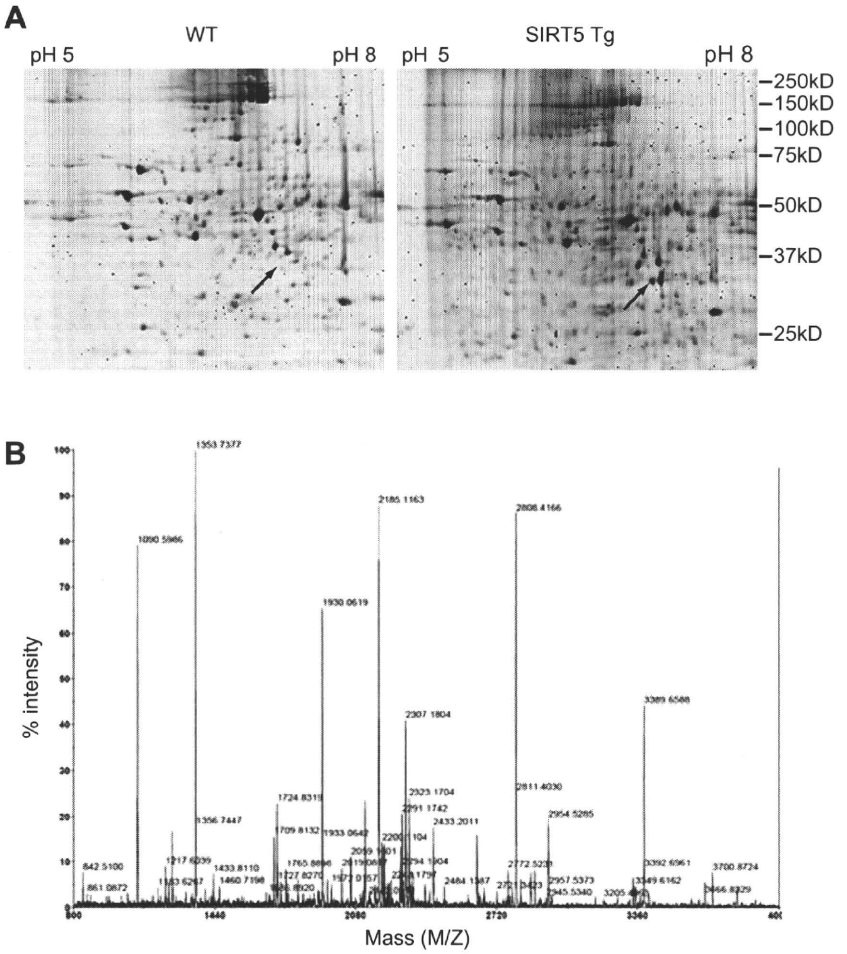

Fig. 3. Identification of the target protein of SIRT5. (A) Two-dimensional electrophoresis of mitochondrial proteins prepared from livers of SIRT5 Tg and wild-type mice. The position of the mitochondrial protein prepared from SIRT5 Tg liver identified by MALDI-TOF-MS is shown by arrow (right panel). The protein is not detected at the corresponding position (indicated by arrow, left panel) in wild-type liver. (B) MALDI-TOF-MS analysis. The mitochondrial protein prepared from SIRT5 Tg liver indicated in (A) was analyzed using MALDI-TOF-MS.

Table 1
Characterization by MALDI-TOF-MS of the target protein of SIRT5.

Measured peptide mass (Da)	Predicted peptide sequence	Start–end
1090.5986	KVPAIYGVDTRM	157–166
1217.6039	KSLGQWLQEEKV	147–156
1353.7377	RGQNQPVLNITNRQ	316–327
1723.8272	KIEFEGQSVDFVDPNKQ	182–196
1930.0619	KEPLFGISTGNIITGLAAGAKS	287–306
2058.1598	RKEPLFGISTGNIITGLAAGAKS	286–306
2184.1154	KGQILTMANPIIGNGGAPDTTARD	90–111
2807.4071	KIEFEGQSVDFVDPNKQNLIAEVSTKD	182–206
2953.5338	KGQILTMANPIIGNGGAPDTTARDELGLNKY	90–118
3662.8010	KMKGYSFGHPSSVAGEVVFNTGLGGYPEALTDPAYKG	55–89

Mass of peptides corresponding to a tryptic digest of CPS1. The corresponding sequence and position (number of amino acid residues) in the sequence are indicated.

expressed predominantly in liver, and catalyzes condensation of ammonia and bicarbonate to carbamoyl phosphate, which is the first step in the urea cycle in liver [15,16].

CPS1 is deacetylated in SIRT5 Tg liver

Since CPS1 is known to be an acetylated protein [26], we investigated deacetylation of CPS1 protein by SIRT5. The mitochondrial protein prepared from livers of SIRT5 Tg and wild-type mice fed *ad libitum* were immunoprecipitated with an anti-acetylated lysine antibody followed by immunoblotting using anti-CPS1 antibody. Acetylated CPS1 protein levels in SIRT5 Tg ($N = 3$) mice were 40% lower than those in wild-type mice ($N = 3$), although total CPS1 expression levels were similar (Fig. 4A). To determine whether SIRT5 protein regulates CPS1 activities, livers of SIRT5 Tg and wild-type mice were homogenized and CPS1 activities were measured. CPS1 activities were significantly increased approximately 2-fold in SIRT5 Tg mice ($N = 5$, $P < 0.01$) compared to those in wild-type mice (Fig. 4B). These results demonstrate that SIRT5 protein deacetylates CPS1 and upregulates its activity in liver.

Urea production is upregulated in SIRT5 Tg hepatocytes

To verify that SIRT5 is involved in the urea cycle by regulating CPS1 activity, production of urea in primary cultured hepatocytes was evaluated. Primary hepatocytes were isolated from SIRT5 Tg and wild-type mice and incubated with ammonia, bicarbonate, and ornithine for 1 h, and the amount of urea synthesized was determined by measuring the urea concentration in the media. Hepatocytes from SIRT5 Tg mice produced more urea than those of wild-type mice (44%, $N = 4$, $P < 0.01$) (Fig. 4C), indicating that urea synthesis is upregulated by overexpression of SIRT5 in liver.

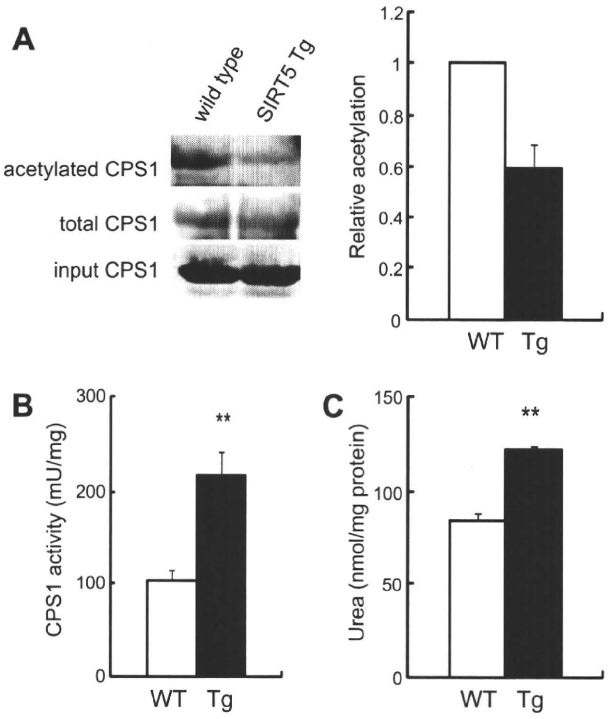

Fig. 4. Deacetylation and activation of CPS1 in livers of SIRT5 Tg mice. (A) CPS1 deacetylation in livers of SIRT5 Tg mice. The mitochondrial protein from livers of SIRT5 Tg and wild-type mice fed *ad libitum* were immunoprecipitated with anti-acetylated lysine antibody (left upper panel) and anti-CPS1 antibody (left middle panel), and immunoblotted with anti-CPS1 antibody. The right panel shows acetylation of CPS1 protein. The ratio of acetylated CPS1 protein of SIRT5 Tg liver to that of wild-type liver was calculated from densitometry of western blots ($N = 3$). (B) Activation of CPS1 activity in SIRT5 Tg liver. Livers of SIRT5 Tg ($N = 5$) and wild-type ($N = 5$) mice fasted for 16 h were homogenized and CPS1 activities were determined as described in Materials and methods. (C) Production of urea in primary cultured hepatocytes. Primary hepatocytes were isolated from SIRT5 Tg ($N = 4$) and wild-type ($N = 4$) mice fasted for 16 h and incubated with $NaHCO_3$ (25 mM), NH_4Cl (10 mM) and ornithine–HCl (5 mM) for 1 h. The amount of urea synthesized was determined by measuring the urea concentration in the media as described in Materials and methods. Values are means ± SEM. $^*P < 0.05$. $^{**}P < 0.01$.

Discussion

In the present study, SIRT5 mRNA levels in liver were found to be increased by fasting. To investigate the function of SIRT5 in liver, we established SIRT5 Tg mice and identified CPS1 as the target protein of SIRT5 by analyses of liver mitochondrial proteins using two-dimensional electrophoresis and MALDI-TOF-MS. We found that CPS1 is deacetylated and that CPS1 activity is significantly increased in the liver of SIRT5 Tg mice. CPS1 is the first and key enzyme of the urea cycle, condensing ammonia with bicarbonate to generate carbamoyl phosphate [15,16]. In hepatocytes from SIRT5 Tg mice, urea synthesis was upregulated compared to that in wild-type mice.

Which residue on CPS1 is deacetylated by SIRT5 is still unclear. The protein that we identified as a target of SIRT5 using two-dimensional electrophoresis and MALDI-TOF-MS was the N-terminal domain of CPS1 (Table. 1), suggesting that the lysine residue of CPS1 deacetylated by SIRT5 is contained in this domain. As Kim et al. reported that CPS1 has nine lysine acetylation sites [26], at least Lys55, Lys119, and/or Lys287 among these lysine residues located in the N-terminal domain might be deacetylated by SIRT5.

During fasting, circulating amino acids, especially alanine, are derived by lysis of muscle proteins, and the amino acids are catalyzed in liver by α-ketoglutarate aminotransferase to generate pyruvate and glutamate. Pyruvate is used in gluconeogenesis to maintain plasma glucose levels, and glutamate is catalyzed by glutamate dehydrogenase to form α-ketoglutarate and ammonia. Ammonia is extremely toxic; the urea cycle converts ammonia to non-toxic urea, which is readily excreted from kidney. It also has been reported that CPS1 activity is increased by fasting or calorie restriction in rodent liver [27,28]. Thus, SIRT5 protein may be involved in detoxification of ammonia during fasting through deacetylation and activation of CPS1.

Recently, Nakagawa et al. reported that CPS1 activity is downregulated in liver of SIRT5 KO mice, which exhibit hyperammonemia by fasting [14]. We show here that CPS1 activity in liver is upregulated in SIRT5 Tg mice during fasting and that urea synthesis is upregulated in SIRT5 Tg hepatocytes, complementing their data.

Suggesting the mechanism of CPS1 activation during fasting, SIRT5 mRNA expression levels in liver were increased by fasting, but protein expression levels were not altered under the same condition in wild-type mice (Supplemental Fig. 1). Nakagawa et al. reported that SIRT5 protein expression levels were not altered, but that NAD levels were elevated by fasting in wild-type mice [14], suggesting that CPS1 is not activated by an increase in SIRT5 protein levels but by activation of SIRT5 through elevation of NAD.

SIRT5 protein is highly expressed in organs other than liver, including kidney, skeletal muscle, and heart (Supplemental Fig. 1), where their functions are yet unknown. Further investigation of the pathophysiological role of SIRT5 is required.

Acknowledgments

This study was supported by Scientific Research Grants from the Ministry of Education, Culture, Sports, Science, and Technology of Japan, from the Ministry of Health, Labor, Welfare, Japan, and by the Kyoto University Global COE Program "Center for Frontier Medicine".

Appendix A. Supplementary data

Supplementary data associated with this article can be found, in the online version, at doi:10.1016/j.bbrc.2010.01.081.

Reference

[1] S. Imai, C.M. Armstrong, M. Kaeberlein, et al., Transcriptional silencing and longevity protein SIR2 is an NAD-dependent histone deacetylase, Nature 403 (2000) 795–800.
[2] M. Kaeberlein, M. McVey, L. Guarente, The SIR2/3/4 complex and SIR2 alone promote longevity in saccharomyces cerevisiae by two different mechanisms, Genes Dev. 13 (1999) 2570–2580.
[3] H.A. Tissenbaum, L. Guarente, Increased dosage of a *sir-2* gene extends lifespan in *Caenorhabditis elegans*, Nature 410 (2001) 227–230.
[4] B. Rogina, S.L. Helfand, SIR2 mediates longevity in the fly through a pathway related to calorie restriction, Proc. Natl. Acad. Sci. USA 101 (2004) 15998–16003.
[5] R.A. Frye, Phylogenetic classification of prokaryotic and eukaryotic SIR2-like proteins, Biochem. Biophys. Res. Commun. 273 (2000) 793–798.
[6] J.T. Rodgers, C. Lerin, W. Haas, S.P. Gygi, et al., Nutrient control of glucose homeostasis through a complex of PGC-1α and SIRT1, Nature 434 (2005) 113–118.
[7] D. Frescas, L. Valent, D. Accili, Nuclear trapping of the forkhead transcription factor FOXO1 via SIRT-dependent deacetylation promotes expression of glucogenetic genes, J. Biol. Chem. 280 (2005) 20589–20595.
[8] Y. Nakamura, M. Ogura, D. Tanaka, et al., Localization of mouse mitochondrial SIRT proteins: shift of SIRT3 to nucleus by co-expression with SIRT5, Biochem. Biophys. Res. Commun. 366 (1) (2008) 174–179.
[9] W.C. Hallows, S. Lee, J.M. Denu, Sirtuins deacetylate and activate mammalian acetyl-CoA synthetases, Proc. Natl. Acad. Sci. USA 103 (2006) 10230–10235.
[10] B. Schwer, J. Bunkenborg, R.O. Verdin, et al., Reversible lysine acetylation controls the activity of the mitochondrial enzyme acetyl-CoA synthetase 2, Proc. Natl Acad. Sci. USA 103 (2005) 10224–10229.
[11] C. Schlicker, M. Gertz, P. Papatheodorou, et al., Substrates and regulation mechanisms for the human mitochondrial sirtuins SIRT3 and SIRT5, J. Mol. Biol. 382 (2008) 790–801.
[12] M.C. Haigis, R. Mostoslavsky, K.M. Haigis, et al., SIRT4 inhibits glutamate dehydrogenase and opposes the effects of calorie restriction in pancreatic beta cells, Cell 126 (2006) 941–954.

[13] B.J. North, B.L. Marshall, M.T. Borra, et al., The human SIR2 ortholog, SIRT2, is an NAD$^+$-dependent tubulin deacetylase, Mol. Cell. 11 (2003) 437–444.
[14] T. Nakagawa, D.J. Lomb, M. Haigis, et al., SIRT5 deacetylates carbamoyl phosphate synthetase 1 and regulates the urea cycle, Cell 137 (2009) 560–570.
[15] M.J. Jackson, A.L. Beaudet, W.E. O'Brien, Mammalian urea cycle enzymes, Annu. Rev. Genet. 20 (1986) 431–464.
[16] J.L. Deignan, S.D. Cederbaum, W.W. Grody, Contrasting features of urea cycle disorders in human patients and knockout mouse models, Mol. Genet. Metab. 93 (2008) 7–14.
[17] J. Miyazaki, K. Araki, E. Yamato, et al., Establishment of a pancreatic beta cell line that retains glucose-inducible insulin secretion: special reference to expression of glucose transporter isoforms, Endocrinology 127 (1990) 126–132.
[18] H. Niwa, K. Yamamua, J. Miyazaki, Efficient selection for high-expression transfectants with a novel eukaryotic vector, Gene 108 (1991) 193–200.
[19] S. Gupta, L.K. Rogers, S.K. Taylor, et al., Inhibition of carbamyl phosphate synthetase-I and glutamine synthetase by hepatotoxic doses of acetaminophen in mice, Toxicol. Appl. Pharmacol. 146 (1997) 317–327.
[20] L.A. Fahien, P.P. Cohen, A kinetic study of carbamyl phosphate synthetase, J. Biol. Chem. 239 (1964) 1925–1934.
[21] M. Hosokawa, B. Thorens, Glucose release from GLUT2-null hepatocytes: characterization of a major and a minor pathway, Am. J. Physiol. Endocrinol. Metab. 282 (2002) E794–801.
[22] D.M. Cyr, S.G. Egan, C.M. Brini, et al., On the mechanism of inhibition of gluconeogenesis and ureagenesis by sodium benzoate, Biochem. Pharmacol. 42 (1991) 645–654.
[23] D. Hunninghake, S. Grisolia, A sensitive and convenient micromethod for estimation of urea, citrulline, and carbamyl derivatives, Anal. Biochem. 16 (1966) 200–205.
[24] W.R. Fearon, The carbamido diacetyl reaction: a test for citrulline, Biochem. J. 33 (1939) 902–907.
[25] S. Nemoto, M.M. Fergusson, T. Finkel, Nutrient availability regulates SIRT1 through a forkhead-dependent pathway, Science 306 (2004) 2105–2108.
[26] S.C. Kim, R. Sprung, Y. Chen, et al., Substrate and functional diversity of lysine acetylation revealed by a proteomics survey, Mol. Cell. 23 (2006) 607–618.
[27] M. Gomez, A. Jorda, J. Cabo, et al., Effect of starvation on the N-acetylglutamate system of rat liver, FEBS. Lett. 156 (1983) 119–122.
[28] J.B. Tillman, J.M. Dhahbi, P.L. Mote, et al., Dietary calorie restriction in mice induces carbamyl phosphate synthetase I gene transcription tissue specifically, J. Biol. Chem. 271 (1996) 3500–3506.